THESIS

INVESTIGATION OF RELBE1 TOXIN-ANTITOXIN FUNCTION IN THE CARBON-

DEPENDENT METABOLIC ADAPTATION OF *MYCOBACTERIUM TUBERCULOSIS*

Submitted by

Julie M. Starkey

Department of Microbiology, Immunology, and Pathology

In partial fulfillment of the requirements

For the Degree of Master of Science

Colorado State University

Fort Collins, Colorado

Summer 2022

Master's Committee:

    Advisor: Richard Slayden

    Karen Dobos
    Zaid Abdo
    Ronald Tjalkens

ABSTRACT

INVESTIGATION OF RELBE1 TOXIN-ANTITOXIN FUNCTION IN THE CARBON-DEPENDENT METABOLIC ADAPTATION OF *MYCOBACTERIUM TUBERCULOSIS*

Tuberculosis (TB) is a devastating disease with suboptimal treatment regimens and a single vaccine with variable efficacy. Reducing the global burden of TB requires a refined arsenal of methods to prevent and treat the disease, which necessitates a better understanding of *M. tuberculosis* (*Mtb*) pathogenesis during infection. *Mtb* undergoes continuous metabolic reprogramming throughout acute and chronic stages of infection in order to survive and persist harsh host conditions, and the regulatory network responsible for mediating metabolic adaptation has not been fully defined. *Mtb* harbors at least 88 Toxin-antitoxin (TA) loci that have been proposed to function as regulatory modules in response to stress. TA systems are uniquely abundant in *Mtb*, making them viable targets for the treatment of both active and latent infection. Several RelBE TA systems are present in *Mtb*, and the RelE toxins function as ribonucleases to inhibit translation when not bound to RelB antitoxins. The genes encoding *relBE1* are adjacent to a gene that encodes an enzyme involved in central carbon metabolism, which could suggest a regulatory role for RelBE1 in carbon metabolism.

We aimed to explore the relationship between the RelBE1 TA system and carbon-mediated metabolic adaptation. This work incorporated *in vitro* transcriptional and genetic studies under defined carbon sources to investigate the activity of RelBE1 and the requirement of RelE1 *in Mtb* metabolism, growth, and viability in the presence of different carbon sources. We observed transcriptional and physiological trends consistent with the hypothesis that RelBE1 contributes to

adaptation of *Mtb* metabolism in the presence of cholesterol and oleate. Additionally, we found evidence that supports the necessity of RelE1 in *Mtb* metabolism under conditions depleted of nutrients. To investigate if multiple RelBE systems work redundantly or cooperatively in *Mtb* metabolic adaptation, we applied CRISPRi to simultaneously silence three RelBE TA loci. CRISPRi construction of knockdown mutants resulted in variable success but did not fully resolve the question regarding the cooperative or redundant functions of RelBE systems in *Mtb* metabolism. Nonetheless, the study provided the building blocks for efficient genetic manipulation of multiple TA systems in *Mtb* that are essential for exploring the coordination of TA systems in their contribution to *Mtb* pathogenesis.

This thesis work contributes to the debate regarding TA system function in *Mtb* stress response and adaptation during infection. Given the limitations of the presented studies, further work is warranted to elucidate the relationship between TA systems and *Mtb* pathogenesis. Expanding our understanding of TA systems in TB disease would provide novel avenues in research to improve treatments against TB.

ACKNOWLEDGEMENTS

TABLE OF CONTENTS

LIST OF TABLES

LIST OF FIGURES

CHAPTER 1: TOXIN-ANTITOXIN SYSTEMS AND METABOLIC ADAPTATION IN
MYCOBACTERIUM TUBERCULOSIS: A LITERATURE REVIEW

1.1 Introduction

Tuberculosis (TB) is an ancient disease, yet it is one of the leading causes of death worldwide due to a single infectious agent. TB affects around 10 million people globally, killing more than one million each year (1). While efforts to control TB disease have been in motion for years, progress is slow and a continuous challenge. The causative agent of TB, *Mycobacterium tuberculosis* (*Mtb*), is a bacterium that has evolved to lay clinically dormant in its human host for up to decades before spreading to the next host. Most individuals infected with TB are able to develop a sufficient immune response to control and suppress *Mtb*, but the immune system often fails to kill all tubercle bacilli in the body (1–7). The bacilli that survive attacks from the immune system undergo persistence, resulting in latent, asymptomatic disease. It can be years before the pathogen finds an opportunity to attack the host and establish active disease (1, 7–9). Current treatments are effective against TB disease but require extensive regimens that often come with adverse side effects (2). Additionally, drug-resistant TB infections are a growing concern, especially in regions of the world with high disease burden (1, 10). Global TB incidence rates have gradually declined over the last century thanks to efforts led by the World Health Organization (1). However, the continual global burden of TB requires further action on all fronts, including the detection, treatment, and prevention of disease.

To better manage TB disease burden and associated fatalities, it is critical to build upon existing knowledge of the pathogen and molecular mechanisms behind *Mtb* pathogenesis. The collective understanding of how *Mtb* establishes disease, evade host immune responses, and

reactivates to cause symptomatic infection allows for the development of novel diagnostic and treatment strategies against active and latent TB disease.

1.2 The History of Tuberculosis: "Captain Among these Men of Death"

Tuberculosis has an extensive history with humans. While many of its *Mycobacterium* relatives are common environmental microorganisms, *M. tuberculosis* has solely relied on humans to survive, replicate, and spread for centuries (11). *Mtb* co-evolved with humans for an estimated 15,000 years and, in that time, adapted a variety of mechanisms to avoid and manipulate host immune defenses to survive (11). While Robert Koch initially characterized the agent in 1882, archeological evidence dates tuberculosis back more than 5,000 years ago in ancient Egypt (12, 13). Throughout the 19th century, TB devastated global populations, particularly children and soldiers, which ignited rigorous studies to understand the disease and its etiology (11). French clinician Jean-Antoine Villemin tested the infectivity of TB in rabbits using infected fluid extracted during an autopsy in 1865, finding obvious signs of infection in the rabbits a few months following inoculation (14). Robert Koch was the first to introduce tuberculin as a diagnostic in 1890 (15), which soon became the standard for detecting TB in patients. By 1907, Clemens Freiherr von Pirquet established intracutaneous injections of tuberculin and subsequent reactions that indicate latent tuberculosis in children (16).

The development of TB diagnostic tools was a step in the right direction for managing TB disease worldwide. TB mortality gradually declined in developing parts of the world as living conditions improved over time (17). Unfortunately, TB cases persisted in younger and older generations, and major wars caused spikes in the number of cases amongst soldiers (18). Countries around the world began developing public health programs to track TB cases within populations and establish resources to treat and prevent infections (11). Sanatoriums were established to house

infected persons, and experimental surgeries attempted to remove and sterilize lungs burdened with tubercle bacilli. Based at the Pasteur Institute in Paris, Albert Calmette and Camille Guérin worked to find a vaccine against TB by attenuating *M. bovis* (19, 20). Their BCG (Bacille Calmette-Guérin) vaccine was ready for clinical testing by 1921 and administered to hundreds of thousands of children across Europe. During World War I, France developed comprehensive public health campaigns in attempt to mitigate the burden of TB in soldiers (21). The first-ever disease control program under the WHO tested 30 million individuals in Europe in 1948 and administered the BCG vaccine in roughly 14 million in the span of a few years (22).

TB-centered committees within the WHO began issuing reports that enacted long-term policies for controlling TB disease and continue to do so today. The WHO declared tuberculosis a global health emergency in 1993, which ignited streamlined funding and resources towards better detecting, treating, and controlling TB disease. The WHO established the End TB Strategy in 2014 with targeted goals of reducing TB incidences and deaths by 80% and 90%, respectively, by the year 2030 (23). Recent reports demonstrate a decrease in disease incidence by roughly 2% per year with a total reduction of 11% since 2015 (1).

Unfortunately, TB continues to decimate populations in developing regions of the world, including India, Africa, and Southeast Asia. Factors such as poverty, overcrowding, and lack of education have been associated with areas of high TB cases (1, 10). Additionally, many developing nations are overwhelmed with other diseases like HIV/AIDS that make individuals more susceptible to TB infections. The recent COVID-19 pandemic especially impacted TB disease control as fewer people had access to TB diagnostics and treatments (1). Despite decades of research, funding, and coordinated efforts to tackle TB on a global scale, we are far from reaching our goals to end the TB epidemic.

1.3 TB Epidemiology

Tuberculosis, a treatable and curable disease, inflicts all regions of the world and affects all age groups. The WHO estimates that about one-quarter of the world population harbors *Mtb* (1). However, only eight countries in the world accounted for two-thirds of the total number of TB cases in 2020, including India, China, South Africa and countries in Southeast Asia (Figure 1).
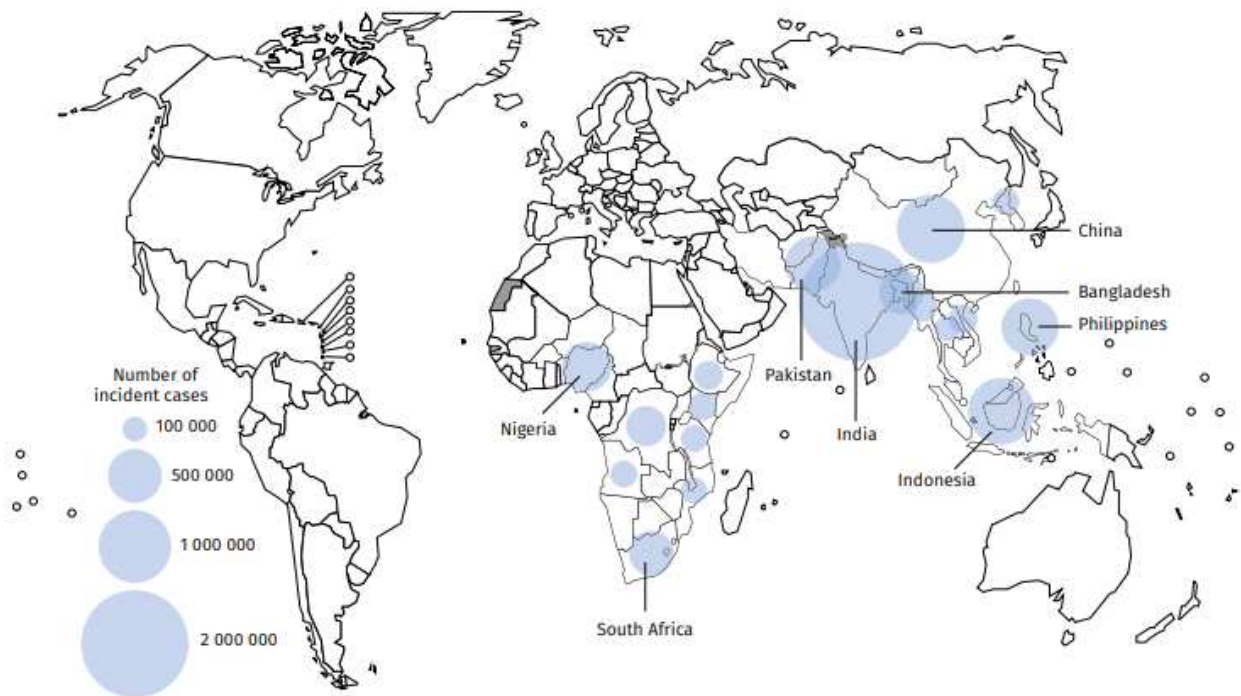
Figure 1.1 2020 TB incidence for countries with highest number of cases. Countries that ranked highest for the number of cases in 2020. Taken from WHO Global Tuberculosis Report 2021 (1).

TB cases continue to put a significant strain on public health services in every country despite low incidence rates in many first-world countries. In 2019 alone, the US recorded 8,916 cases and estimated that 13 million people are living with latent TB (24).

TB is acquired by aerosolizing *Mtb* from an individual with active disease. Persons with active TB transmit *Mtb* bacteria via aerosols produced when speaking or coughing, which

contributes to the overall transmission of TB. *Mtb* primarily infects the lungs and causes pulmonary disease, but the pathogen can spread to other regions of the body, including the brain and kidneys (2). Common symptoms of pulmonary TB include coughing, chest pain, weight loss, and fever. However, a majority of those infected with *Mtb* develop latent TB infection (LTBI) that does not produce any symptoms. LTBI thus does not result in the spread of *Mtb* but can be fatal if not properly treated. Individuals with LTBI have a 5-10% chance of developing active disease at some point in their lives that increases with the presence of preexisting conditions or other risk factors (2).

External factors like occupational risks, malnutrition, alcohol use, and smoking increase the risk of acquiring TB (1, 2, 24). Weakened immune systems, which occur naturally with age, can also lead to the development of active TB disease in infected individuals. Medical conditions, including diabetes, chronic infections, and cancers, often result in compromised immune systems that have a harder time fighting off TB infections. HIV-infected individuals are 18 times more likely to contract TB, and without proper treatment, mortality rates from the co-infection is extremely high (24).

1.4 Treatment of Active and Latent TB

Over 66 million lives have been saved by TB management efforts from 2000 to 2020, but the WHO estimates that one-third of all infected individuals do not get diagnosed in time to receive proper treatment (1, 2). Some of the many challenges in tackling the TB epidemic revolve around this large percentage of cases. Treatment of tuberculosis involves the use of first-line antibiotics over the course of six to nine months: isoniazid (INH), rifampin (RIF), ethambutol (EMB), and pyrazinamide (PZA). Treatment regimens may vary depending on the stage of disease and individual's health status (25). LBTI treatment can also incorporate rifapentine (RPT) and short-

course regimens to reduce toxicity in patients (26). Anti-TB drugs possess moderate side effects and toxicity levels that often lead to noncompliance of regimens by patients.

Frequent use and mismanagement of TB antibiotics over time has contributed the rise of drug resistant *Mtb* strains that require alternative treatments. *Mtb* strains classified as multidrug-resistant TB (MDR TB) present resistance to the most effective drugs, INH and RIF. Fluoroquinolones can be substituted for treatment of MDR TB, but serious adverse reactions are common and not recommended for those with other treatment options available (27). Although rare, extensively and extremely drug-resistant TB (XDR/XXDR TB) has developed over the last few decades in which the patient does not respond to treatment of most anti-TB drugs, including INH, RIF, fluoroquinolones, and common second-line antibiotics like kanamycin (28). XXDR TB strains present resistance to all current first- and second-line TB drugs. Countries with high TB burden experience more cases of drug-resistant TB that contribute to the transmission of untreatable strains around the world (2). Few cases of XDR TB have been reported in the US, but those numbers could increase with the continued prevalence of TB worldwide (1). The steady rise of multidrug resistance in *Mtb* increases the need for more effective yet accessible treatment options. Research continues to pursue the optimization existing drugs and develop efficient drug discovery pipelines to help establish improved treatment regimens that are effective against all strains of *Mtb* (1, 2).

The BCG vaccine stands as the only licensed vaccine available for preventing TB disease. While the vaccine helps prevent the development of active TB in newborns, efficacy in adults is more variable for unknown reasons. Previous studies have reported a decline in protection in children as they age following vaccination (29, 30). The BCG vaccine is thus widely implemented in high TB burden countries but not offered in countries with low case rates, including the US.

Regardless, the BCG vaccine provides substantial evidence that vaccine-mediated protection against TB is achievable. In addition to improving TB treatment, ongoing studies aim to develop a novel vaccine effective against both active and latent TB. One vaccine currently being tested is VPM1002, a live vaccine candidate that functions to broaden the adaptive immune response to *Mtb* (20). This candidate has been shown to stimulate CD8+ lymphocytes, CD4+ TH1, and memory T cells specific to the mycobacterial antigen, Ag85B. Positive findings have been reported in preclinical models compared to BCG in conjunction with the completion of phase I-II trials in South Africa (20).

1.5 Challenges of the TB Epidemic

The COVID-19 pandemic has significantly dampened global efforts to control tuberculosis as it stretched public health facilities, resources, and services thin since its arrival in early 2020. The WHO reports that an 18% drop in TB diagnosis worldwide followed the onset of the pandemic. Due to struggles in controlling the spread of COVID-19, India had the largest reduction in the number of reported TB cases, accounting for over 40% of the global decline in notifications (1). Fewer reported cases globally indicates that fewer patients are getting the proper treatment and more people are facing increased risks of TB-related death.

The WHO set the goal to have TB rates under control by 2030, but several hurdles currently stand between us and TB eradication: (1) undiagnosed LBTI cases that go untreated, (2) a rise in drug resistance that decreases the efficacy of current treatments, (3) a vaccine with suboptimal efficacy in adults, (4) a lack of appropriate and consistent funding and resources, and (5) gaps in knowledge surrounding the disease. Goals established by the WHO in their End TB Strategy may be reached over the next decade if the current issues can be efficiently addressed. Despite decades of extensive research, scientific understanding of the underlying mechanisms of TB disease is

lacking insight critical to effectively tackle the TB epidemic. Numerous questions regarding *Mtb* pathogenesis and TB immunity remain, and efforts to improve TB treatment and prevention require extensive comprehension of this complex disease.

1.6 Mechanisms of TB Disease

When an individual is exposed to *Mtb*, the bacilli enter their host via the respiratory tract and colonize the lungs. Various cells that encounter the invading bacteria, immune or otherwise, elicit responses to activate the host's innate immune defenses. In about 90% of individuals exposed to TB, the immune response is effective in initially suppressing the proliferation of *Mtb*. Alveolar macrophages and other phagocytes activated by pro-inflammatory cytokines like IFN-γ engulf the invading bacteria and initiate intracellular responses that target and kill the pathogen. However, *Mtb* can survive macrophage-driven attacks and persist within the host. *Mtb* virulence revolves around transmission and thus harbors various mechanisms essential for immune evasion and modulation of the bacterium's own cellular processes that enable long-term survival (31). For instance, secretion systems expressed by the pathogen can help prevent the toxicity of volatile compounds or modulate the macrophage's immune phenotype. *Mtb* also possesses various regulators that control the expression of factors involved in stress adaptation, nutrient uptake, and avoiding host immune attacks (32). The evasion of phagocytic defenses elicited by the host allows *Mtb* to replicate and disseminate, eventually reaching the local draining lymph node that further stimulates adaptive immune responses.

The host immune system attempts to combat the spread of infection by directing various immune cells to localized regions with the lung that ultimately form granulomas (6, 33–35). These granular regions trap *Mtb* in an aggregate of macrophages and lymphocytes following activation by TNF-α and prevent dissemination of bacteria to the rest of the body (35, 36). *Mtb* bacteria often

persist within granulomas, even as they face nutrient starvation, oxygen depletion, and lowered

pH (Figure 1.2). Transcriptional studies of *Mtb* have long established that the bacterium undergoes

transcriptional reprogramming to improve metabolic efficiency in low-nutrient environments and

produce proteins that aid in host immune modulation (34, 37–39). Over time, the granuloma can

necrotize and eventually fail to contain *Mtb,* allowing the pathogen to re-initiate growth following

extended periods of persistence. This sequence of events result in active disease, in which bacteria

are expelled from the lungs and transmitted to the next host (7, 9).
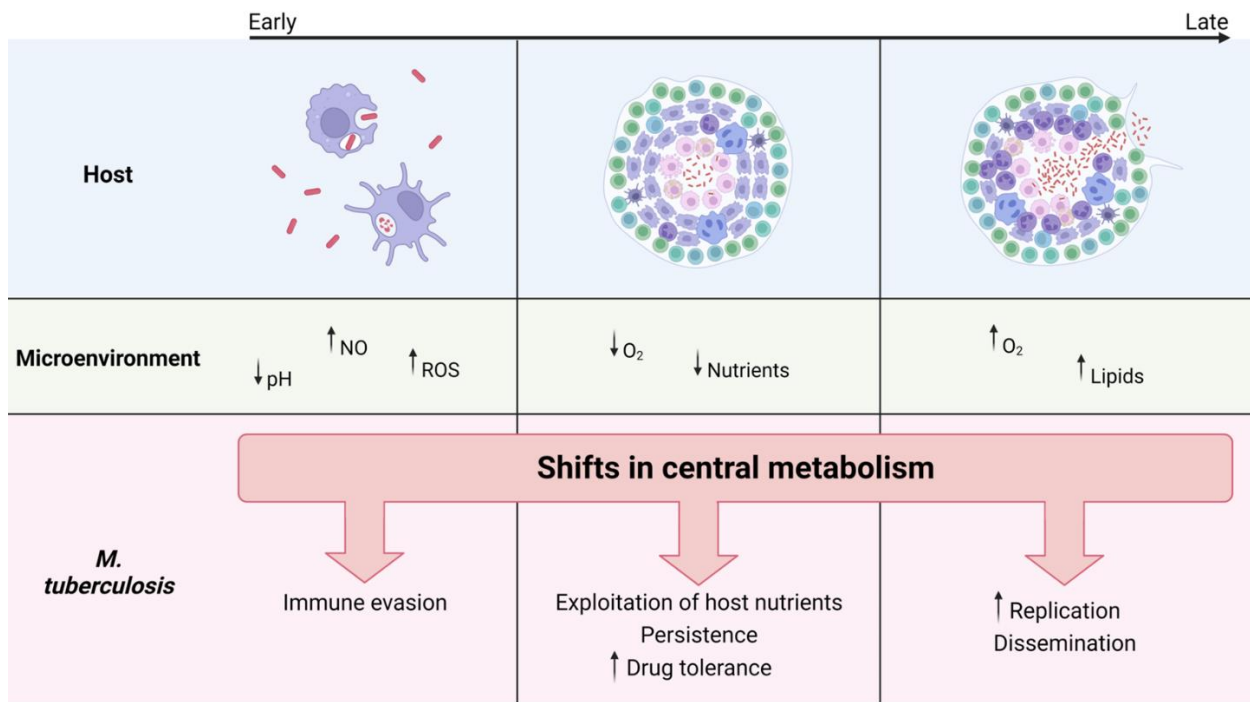
Figure 1.2 *Mtb* adaptation to host-mediated microenvironments during infection. At different stages of TB infection, host immune responses to *Mtb* result in microenvironments that are typically lethal to microbial pathogens. *Mtb* has evolved to navigate and survive these conditions by continuously reprogramming its metabolic network. Metabolic adaptation allows *Mtb* to initiate molecular mechanisms that aid in evading host immune responses, establish persistence, and eventually escape granulomas. Figure created with Biorender.com.

1.7 *Mtb* Adaptation to its Host

Mtb evolved to adapt to the stringent host conditions encountered during infection and take

advantage of resources provided by the host to survive, persist, and eventually move on to its next

host (40). For instance, *Mtb* relies on its unique cell envelope to tolerate and resist antibiotic exposure. Its elaborate cell envelope composed of peptidoglycan, mycolic acids, and other lipid structures harbor a range of proteins essential for *Mtb* pathogenesis (40–42). Some proteins manipulate the permeability of the cell wall following antibiotic exposure, and others are intricately involved in the direct inactivation of various drugs like INH (43, 44). Components of the *Mtb* envelope, including the ESX type VII secretion system, have been implicated in arresting phagosome acidification and other immunomodulatory activities (45).

The key to successfully surviving the host environment as a pathogen is to acquire nutrients essential for growth and replication. Broad transcriptional reprogramming that allows the pathogen to adapt to growth-restrictive microenvironments during infection has been repeatedly characterized in *Mtb* (7, 38, 40, 46–49). *Mtb* has been shown to require numerous metabolic enzymes for survival under *in vitro* stress conditions and *in vivo*, suggesting that metabolic modulation is critical for persistence during infection (47, 50–55). A collection of evidence suggests that *Mtb* primarily relies on cholesterol and fatty acids as carbon and energy sources during infection (47, 56–59). Interestingly, a combination of metabolite labeling and genetic studies support the hypothesis that *Mtb* can take up different carbon sources and shunt the substrates through the appropriate pathways concurrently towards different metabolic fates (60). This finding led to an alternative hypothesis that *Mtb* does not solely rely on lipid and fatty acids as carbon sources throughout infection (61, 62). Serafini and others argued that *Mtb* likely takes up lactate and pyruvate since they're abundant in human cells during inflammation. Their work revealed that lactate and pyruvate metabolism produces propionyl-CoA, which is essential for synthesizing odd-chain fatty acids comprising the cell envelope (62). The unusual nature of carbon

utilization in *Mtb* relative to other bacterial pathogens points to metabolic adaptation as a critical component for pathogenesis throughout infection.

Given that *Mtb* must continually adapt its metabolism in response to dynamic host stresses throughout infection, defining the regulatory mechanisms responsible for metabolic reprogramming are key to understanding overall persistence and pathogenesis. For instance, work by Abramovitch's research group has shown that growth arrest in low pH conditions depends on the carbon sources available, which is controlled by the two-component regulatory system, *phoPR* (54). Studies in *E. coli* and other intracellular pathogens have described the importance of the signaling molecule, (p)ppGpp, in mediating metabolic reprogramming under stress (63–65). *Mtb* likely relies on Rel$_{Mtb}$ (Rv2583c) to metabolize (p)ppGpp and initiate the stringent response, characterized by altered metabolomic networks following nutrient starvation, that enables long-term survival during infection (63, 66). Given the variety of stresses and microenvironments *Mtb* encounters throughout infection, there are likely vast networks of regulatory mechanisms essential for *Mtb* persistence that have yet to be characterized.

1.8 Toxin-Antitoxin Systems

Many prokaryotes, particularly pathogenic *E. coli*, *Pseudomonas aeruginosa*, *Listeria monocytogenes*, and *Mycobacterium tuberculosis* possess various molecular tools to enhance their growth and survive otherwise lethal conditions (67). Toxin-antitoxin (TA) systems are one of many virulence factors that have been of great interest when dissecting bacterial pathogenesis (68, 69). TA systems consist of a protein toxin and a cognate (RNA or protein) antitoxin that neutralizes the toxin's activity. Often referred to as "poison-antidote" gene pairs, TA systems are ubiquitous in prokaryotes and possess a diverse range of types and proposed biological functions (68–70).

The first TA system was discovered in *E. coli* and found to stabilize plasmids via post-segregational killing in which cells that do not possess the plasmids encoding the TA system were killed (71). Over time, thousands of putative TA systems were discovered, both on plasmids and chromosomes, in numerous prokaryotes. Many characterized TA systems encode toxins with biochemical functions that target integral structures or pathways involved in cell replication, transcription, and translation (68). TA systems are typically encoded within a single operon, but toxin proteins are generally more stable than their antitoxin counterpart. Thus, antitoxins are preferentially degraded by proteases or RNases under certain conditions (68, 72). Degradation of the antitoxin allows the cognate toxin to elicit its activity on the cell until conditions favor the production of antitoxin to neutralize the cognate toxin.

TA systems are grouped into eight types based on the toxin's biochemical activity and the antitoxin's neutralizing mechanism (Figure 1.3). Some types of TA systems, including type II and III systems, involve antitoxins physically interacting with their cognate partner to inhibit toxin activity (73). However, antitoxins belonging to other types of TA systems use different mechanisms of toxin inhibition (Figure 1.3). Type II TA systems are the most extensively studied due to their prevalence in *E. coli* and common bacterial pathogens. Both the toxin and antitoxin are proteins that interact, forming an inert protein complex. The antitoxin additionally possesses a DNA-binding domain that allows it to autoregulate the TA operon. TA protein complexes also influence the TA operon's transcription, and the stoichiometric ratio of antitoxin to toxin within the TA protein complex defines the level of transcriptional repression (74). Known as conditional cooperativity, it is thought that this mechanism allows for controlled production of TA systems under dynamic environmental conditions (68, 75, 76).
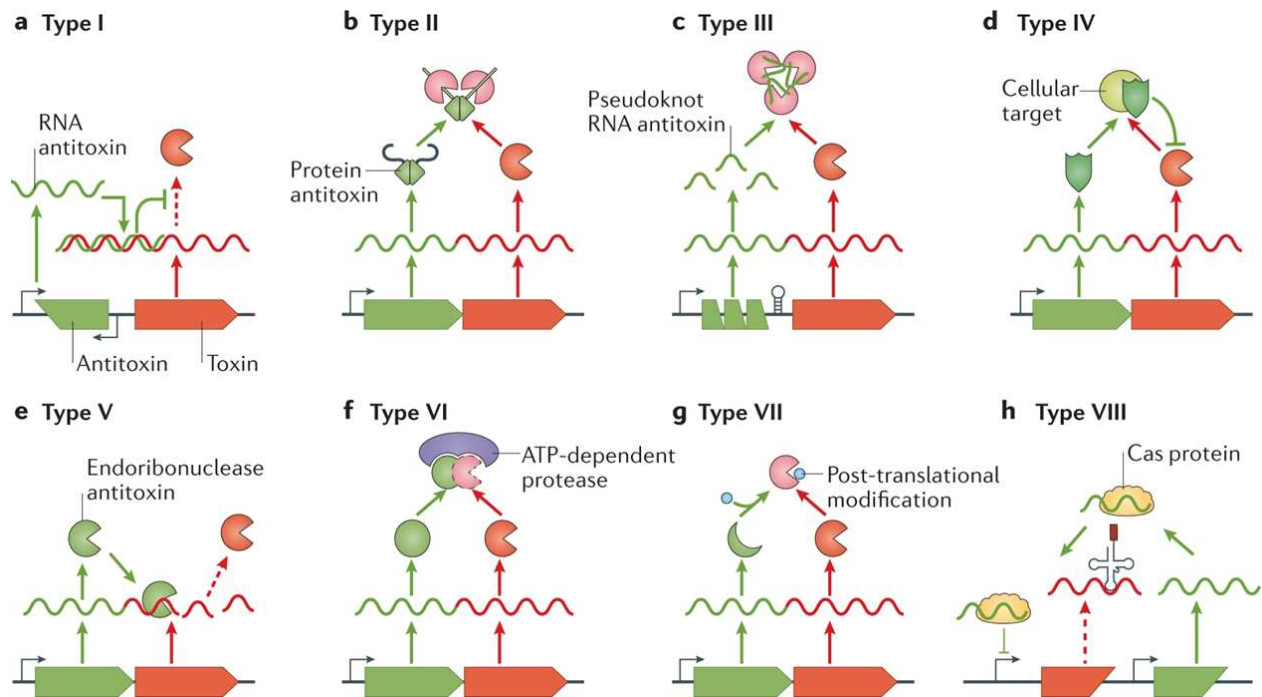
Figure 1.3 Toxin-antitoxin systems in prokaryotes. Different types of TA systems defined by toxin activity and antitoxin mechanisms of regulation. (a) Type I systems incorporate an RNA antitoxin that interacts with toxin mRNA to inhibit the translation of the toxin. (b) Type II systems involve a protein antitoxin that physically binds to the toxin. (c) Antitoxins in type III systems exist as RNA molecules that interact with toxins to inhibit its activity. (d) Type IV antitoxins interact with the targets of the toxin to prevent toxin binding. (e) Antitoxins in type V systems cleave mRNA encoding the toxins to prevent toxin translation. (f) Type VI systems possess antitoxins that interact with toxins and promote targeted degradation by proteases. (g) Antitoxins from type VII systems inhibit toxin activity via post-translational modifications. (h) Type VIII TA systems encode RNA antitoxins that use Cas proteins to target toxins for transcriptional repression. Taken from Jurénas *et al.* 2022 (73).

Numerous type II TA systems have been associated with bacterial persistence and response to stress conditions. Many toxins have been shown to induce growth arrest or cell dormancy when not inhibited by its cognate antitoxin (69, 77). While previous studies have provided evidence of TA systems contributing to genome stabilization, defense against phages, and persister cell formation, there is still debate surrounding the true roles of these systems in stress response and persistence. Previous studies have developed mutants with multiple TA system deletions, but follow-up work with these strains have yielded contradictory results (78–80).

13

1.9 TA Systems in *Mycobacterium*

Species of *Mycobacterium*, mostly members of the *Mycobacterium tuberculosis* complex (MTBC), harbor TA systems (81). Unlike most prokaryotes carrying TA systems, *Mtb* possesses a highly expanded repertoire of chromosomal TA systems. Up to 88 TA systems have been identified in *Mtb*, either through biochemical studies or bioinformatic predictions (81, 82). This expansion of TA systems is not observed in mycobacteria outside of the MTBC, including non-tuberculosis mycobacteria that can cause infections in immunocompromised individuals (Figure 1.4). It is thought that TA expansion occurred with or after the diversion of the MTBC, and a growing collection of evidence points to TA systems being intricately involved in *Mtb* pathogenesis (81, 83–87).
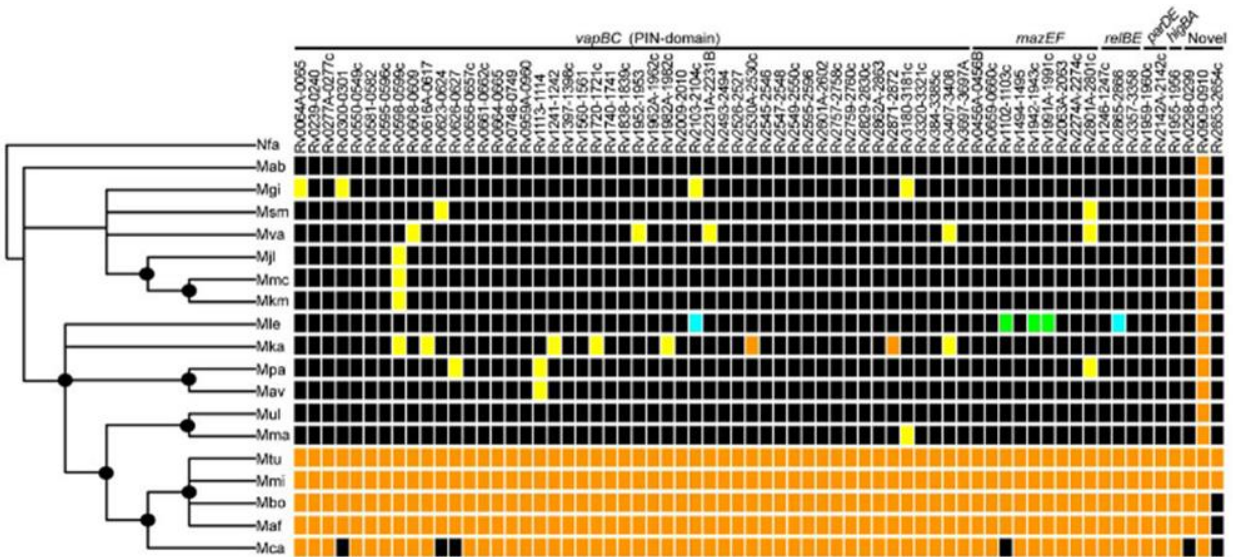
Figure 1.4 Conservation of toxin-antitoxin systems across the *Mycobacterium* genus. Phylogenetic tree showing TA system conservation in species of *Mycobacterium* with *Nocardia farcinica* (Nfa) as the outgroup. TA systems are arranged according to family. Orange = orthologs; yellow = homologs; blue/green = pseudogenes residing in similar/different genomic contexts; black = no BLAST hits. Taken from Ramage *et. al* 2009 (81).

Most TA loci fall under Type II systems, which includes the VapBC, MazEF, and RelBE families. While *Mtb* harbors dozens of VapBC and MazEF loci, only five RelBE loci have been identified (two additional loci were detected using computational analysis but have not been experimentally confirmed) (81, 88). RelE toxins function as ribosome-dependent ribonucleases that selectively cleave coding RNA when not bound to antitoxins (89, 90). RelB antitoxin proteins directly interact with RelE toxins to inhibit the toxin's biochemical activity and autoregulate further transcription of the *relBE* operon (Figure 1.5). Under conditions that promote the activity of Clp or Lon proteases, RelB proteins are preferentially degraded. Targeted degradation of RelB induces RelE activity and transcription of *relBE*. Stoichiometric ratios of RelB and RelE proteins defines the level of regulation: a low RelE:RelB ratio enables the binding of RelB to the operon, while a high ratio changes the conformation of the RelB DNA-binding domain and results in the release of the complex from the operon (75, 76).
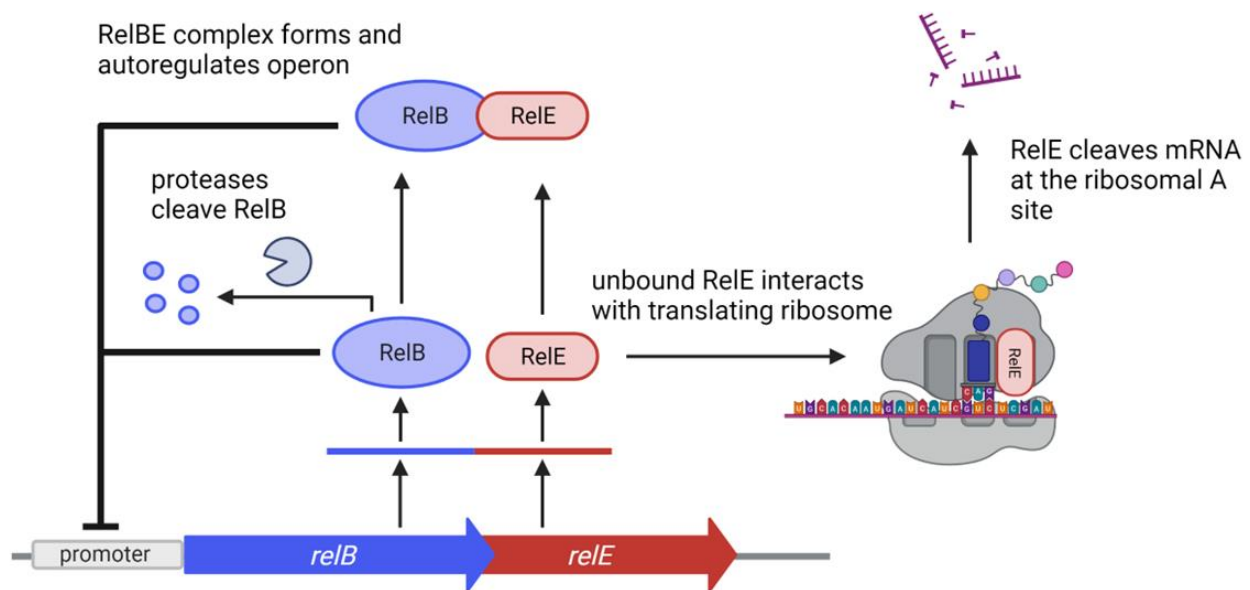
Figure 1.5. Schematic of RelBE toxin-antitoxin system function and interactions. Genes encoding *relB* and *relE* comprise a single operon. RelB and RelE proteins are translated and interact to inhibit RelE activity and negatively regulate expression of the operon. Stress-induced proteases can cleave RelB antitoxins, allowing RelE toxins to undergo ribosome-dependent mRNA cleavage. Figure created with Biorender.com.

Previous work detected transcriptional activity of a select number of *Mtb* TA systems under *in vitro* stress conditions (81, 87, 88). However, most studies rely on toxin overexpression and transcription to make the argument that TA systems play a role in pathogenesis. No current *Mtb* research shows evidence of the native production and activity of toxin proteins following stress exposure or the cooperation of numerous systems in *Mtb* persistence or virulence. Such evidence is essential to claim TA systems directly *Mtb* pathogenicity. Foundational studies of RelBE TA systems in *Mtb* observed translation inhibition and global proteomic changes following the overexpression of RelE toxins (87–89). Specific *in vitro* stresses have been previously shown to induce transcriptional activity of *relBE1*, *-2*, and *-3*, but their precise roles in *Mtb* growth and survival during infection have yet to be fully characterized.

The bi-cistron encoding RelBE1 (Rv1246c-1247c) is adjacent to Rv1248c, a multi-functional alpha-ketoglutarate decarboxylase (Kgd) required for *Mtb* survival. This genomic organization suggests potential involvement of RelBE1 in the adaptive regulation of metabolism in response to changes in carbon availability. Other instances of "regulator-regulated gene neighbors" have been observed in *Mtb*, including members of the VapBC TA family and MadR1, a cell cycle regulator genomically adjacent to an enzyme involved in pyruvate catabolism (91). Given (1) the large number of TA systems in *Mtb*, (2) the critical importance of adaptation to stress during infection, and (3) the current debate regarding TA system function, it is essential to thoroughly assess their potential roles in pathogenesis.

1.10 Thesis Objectives

Due to the prevalence of TA systems in *Mtb*, we hypothesize that TA systems, including RelBE1, contribute to *Mtb* adaptation to stresses like nutrient limitation during infection. This thesis aims to investigate the relevance of the RelBE1 TA system in *Mtb* metabolic adaptation

following exposure to defined carbon sources. RelBE1 is hypothesized to differentially regulate *Mtb* adaptation to carbohydrate and glycolytic versus cholesterol and fatty acid carbon sources. A combination of transcriptional, genetic, and physiological studies were implemented to elucidate carbon source dependent *relBE1* expression and function in *Mtb*. Additionally, we sought to utilize CRISPRi gene silencing to knock down the expression of *relBE1*, *relBE2*, and *relBE3* simultaneously as a technique to dissect potential the cooperation or functional redundancy of TA systems in *Mtb*.

Defining the roles RelBE1 play in *Mtb* adaptation and persistence will bridge significant gaps in knowledge regarding the biological relevance of TA systems in *Mtb* pathogenesis. The research described here can help to answer why *Mtb* uniquely possesses such an extensive repertoire of TA systems, one of the most pressing questions in the field of TA systems. TA systems pose as novel targets for treatment against tuberculosis and other prokaryotic pathogens that harbor TA systems, but first we must understand how they contribute to the pathogenic traits observed during infection.

CHAPTER 2: CHARACTERIZION OF RELBE1 IN THE CARBON-MEDIATED
ADAPTATION OF *MYCOBACTERIUM TUBERCULOSIS*

2.1 Introduction

Tuberculosis persists within the human population as one of the deadliest infectious diseases despite decades of research and public health initiatives. The success of *Mtb* stems from the pathogen's ability to adapt and survive stringent conditions elicited by the host for extended periods (92–95). Intracellular bacilli must survive the engulfment of macrophages and other phagocytes early on during infection, and the remaining bacteria during later stages of disease have to endure the stringent and dynamic extracellular environments within necrotic granulomas (7, 95–98). *Mtb* likely experiences stressful conditions, including nutrient limitation, low pH, hypoxia, and antibiotic treatment, during infection. Depending on the physiological conditions present, the pathogen either rapidly divides to disseminate throughout the host or enters a state of non-replicative persistence that ensures long-term survival (7, 92, 93). The ability to undergo metabolic reprogramming and adaptation is critical to *Mtb* survival the ever-shifting host microenvironment throughout infection (40, 46, 99–101).

Given *Mtb*'s restricted ecological niche, it's not surprising that the pathogen has evolved unique strategies to navigate and adapt to stress conditions elicited by its host. Key pathways and enzymes in carbon metabolism have been demonstrated for *Mtb* survival under stress conditions and virulence (53, 96, 100, 102, 103). Under low pH conditions, Baker and others found that some carbon sources, including pyruvate and cholesterol, enable *Mtb* growth *in vitro*, while other substrates, like glycerol and lactate, result in non-replicating persistence (54). The tricarboxylic acid (TCA) cycle is positioned in the center of carbon metabolism and provides the bacterium with

NADH along with lipid and amino acid precursors. *Mtb* possesses an enzyme within the TCA cycle termed alpha-ketoglutarate decarboxylase (Kgd) rather than the traditional alpha-ketoglutarate dehydrogenase found in other organisms. Kgd is proposed to offer an alternative pathway for synthesizing succinate under stringent conditions (52, 104).

Within the TCA cycle lies the glyoxylate shunt, which functions as a shortcut for carbon metabolism when the organism relies on fatty acids instead of carbohydrates for growth. Lipids have long been proposed as primary carbon sources for *Mtb* during infection, and studies point to cholesterol utilization as a key factor for persistence (37, 47, 57, 105–107). The first enzyme of the glyoxylate shunt, isocitrate lyase (Icl), was previously shown to be required for the persistence and virulence of *Mtb in vivo*, particularly during latent infection (51, 108). Interestingly, *Mtb* mutants lacking *icl* were attenuated in immune-competent mice yet lethal in IFN-$\gamma^{-/-}$ mice (51). Additionally, *Mtb* has been uniquely shown to co-catabolize substrates rather than sequentially utilizing carbon sources (60, 109). Given these findings, some studies argue that carbohydrates and glycolytic products are important carbon substrates during infection (62, 101). Lactate and pyruvate metabolism rely on the glyoxylate shunt and methylcitrate cycle, both of which require Icl. The methylcitrate cycle was found to function in reverse for *Mtb* to metabolize lactate and pyruvate efficiently (62).

While *Mtb* metabolism has been extensively studied, the regulatory mechanisms underlying metabolic adaptation under clinically relevant stress conditions have yet to be fully elucidated. Griffin *et al.* demonstrated in a 2012 study the requirement of *Rv1129c* in the growth of *Mtb* with cholesterol as a single carbon source, which regulates the genomically adjacent genes, *prpD* and *prpC*, involved in the methylcitrate cycle (47). Additionally, *Mtb* was shown to regulate growth in the presence of certain carbon sources in low pH conditions using the *phoPR* two-

component system, leading to metabolic reprogramming and increased virulence *in vivo* (54). Even with the growing evidence of metabolic regulatory mechanisms, *Mtb* and other pathogenic members of the *Mycobacterium tuberculosis* complex (MTBC) possess other regulatory elements that may play pivotal roles in stress response and metabolic reprogramming. *Mtb* harbors a particularly extensive and elusive repertoire of small genetic elements known as toxin-antitoxin (TA) systems.

Mtb possesses at least 88 stable TA loci in its genome, suggesting that they likely play critical functions in pathogenicity (69, 81). A majority of the pathogen's repertoire consists of type II systems, including members of the MazEF, VapBC, and RelBE families. The RelE toxin, when not inhibited by the RelB protein antitoxin, functions as a ribonuclease to establish translation inhibition (89, 110). Previous studies have revealed that *relBE* loci are transcriptionally activated following exposure to stress, and the overexpression of *relE* toxins results in global proteomic changes and bacterial growth arrest (87, 88, 110). Interestingly, the genes encoding *relBE1* (*Rv1246c-47c*) are adjacent to the gene that encodes Kgd (*Rv1248c*). Since TA systems are proposed to function as stress response modules in *Mtb*, we hypothesize that RelBE TA systems contribute to metabolic adaptation during infection by regulating *kgd* expression in the presence of lipids.

This study explores the role of the *relBE1* TA system in the metabolic and physiological response of *Mtb* to carbon source exposure. Differences in bacterial transcription, growth, and viability following exposure to different carbon sources were assessed between wildtype (WT) *M. tuberculosis* and *MtbΔrelE1*. RelBE1 is hypothesized to demonstrate differential expression in the presence of different carbon sources and be required for survival in lipid conditions. If RelE1 functions to negatively regulate *kgd* in the presence of lipids or fatty acids, RelE1 toxins

presumably (1) regulate *kgd* via transcriptional coupling or (2) cleave neighboring *kgd* transcripts to help shift the carbon flow through the glyoxylate shunt of the TCA cycle. *Mtb* TA systems would be promising targets for novel therapeutics against TB and other pathogens that harbor TA systems. Thus, gaining further understanding of TA systems in relation to *Mtb* survival under stringent conditions encountered during infection is critical for advancing our efforts to control TB disease worldwide.

2.2 Methods and Materials

2.2.1 Bacterial Strains and Experimental Growth Conditions

WT *M. tuberculosis* H37Rv and *MtbΔrelE1* were used in the present study. *MtbΔrelE1* is a complete deletion of the *relE1* gene via allelic exchange previously generated in the Slayden laboratory. *Mtb* liquid cultures were maintained in 7H9 Middlebrook medium supplemented with 10% OADC and 0.05% Tyloxapol (Tylox, Sigma-Aldrich) and incubated at 37°C with constant shaking at 200rpm. Liquid and solid media were supplemented with Kanamycin (Kan, 25µg/mL) for the growth of *ΔrelE1*. All culture work was performed in the Biosafety Level 3 (BSL-3) laboratory in accordance with CSU Biosafety regulations and procedures.

Defined carbon condition experiments were performed in 7H9+OADC+Tylox or minimal medium (MM) prepared as described previously (54, 58): 1 g/L KH2PO4, 2.5 g/L Na2PO4, 0.5 g/L (NH4)2SO4, 0.15 g/L asparagine, 10 mg/L MgSO4, 50 mg/mL ferric ammonium citrate, 0.1 mg/L ZnSO4, 0.5 mg CaCl2, and 0.05% Tyloxapol. Concentrations of carbon sources were based on literature assessing carbon-dependent growth arrest under low pH (54). Mid-to-late log *Mtb* was used to inoculate defined carbon media at an initial optical density at 600nm (OD_{600}) of 0.2-0.3. Briefly, cultures were centrifuged at 3,500rpm for 10 minutes, washed once with 1X TBST to

remove residual medium, and resuspended in the defined carbon condition. Cultures were incubated at 37°C, shaking at 200rpm, and growth was monitored using OD_{600} measurements over the course of six days. Every 48 hours, samples from each growth culture were serially diluted to 10^{-6} in 1X TBST and plated onto 7H11 or 7H10+Kan quad plates. Plates were incubated at 37°C for 21-28 days until colony forming units (CFUs) were visible. Enumerated CFUs were used to calculate CFU/mL for each timepoint. Significance between genotypes was identified using mixed model ANOVA with Tukey's multiple comparisons, with p-values from pairwise comparisons listed in Table S2.3B, C.

2.2.2 *Mtb* Total RNA Extraction and Purification

Following 1- and 24 hours of carbon source exposure, 50mL of each *Mtb* culture were pelleted at 3,500rpm, 4°C for 10 minutes and resuspended in 1mL TRIZol Reagent (Invitrogen). Cells were mechanically lysed with 0.1mm zirconia beads (BioSpec Products) using the Mini BeadBeater (BioSpec Products) for a total of four rounds of 30-second intervals with 2-minute incubations on ice. Samples were stored at -80°C until RNA extractions. Frozen sample tubes were treated with appropriate tuberculocidal disinfectant according to manufacturer procedures and transferred out of the BSL3 laboratory for further experimentation.

Total RNA was extracted using chloroform-phenol according to established TRIzol protocols and underwent two rounds of DNAse treatment. Briefly, 200µL chloroform (Sigma) was added to lysed samples and mixed by vortexing. Samples were centrifuged at 12,000xg, 4°C for 15 minutes. The aqueous layers were transferred to new tubes containing 500µL isopropanol (Sigma) and 0.5µL glycogen (Thermo Fisher), and samples were incubated at -20°C overnight. Total RNA was pelleted at 12,000xg, 4°C for 10 minutes and washed once with 80% ethanol. RNA samples were treated with ten units of DNase I (Thermo Fisher) at 37 °C for 60 minutes. 100µL

phenol:chloroform:isoamyl alcohol (Sigma Aldrich) was added to treated RNA. Samples were vortexed briefly and centrifuged at 12,000xg, 4˚C for 10 minutes. Aqueous layers were transferred to new tubes containing 450µL 10% ammonium acetate, 80% ethanol and 0.5µL glycogen and stored at -20˚C overnight. DNase-treated RNA was washed with 80% ethanol, pelleted, and resuspended in 50 µL DEPC water. Total RNA quantities and qualities were measured using the Qubit Fluorometer and Nanodrop, respectively.

2.2.3 Reverse Transcription- and Reverse Transcription-Quantitative PCR

cDNA was generated from 1µg total RNA and random hexamer primers using the FirstStrand cDNA Synthesis Kit (Roche) according to manufacturer instructions. Reverse transcription PCR (RT-PCR) was performed on WT *Mtb* H37Rv cDNA using qPCR gene-specific primer sets (either alone or in combination, Table S1). *Mtb* gDNA and no template control reactions were included in RT-PCR reactions. Amplicons were visualized using agarose gel electrophoresis and staining. Briefly, PCR products were diluted in 6X Loading Dye (Thermo Fisher), loaded into a 1% agarose gel, and electrophoresed at 80V for 90 minutes. The gel was stained with SYBR Gold Nucleic Acid Stain (Thermo) and visualized using the BioRad Chemi-Doc Imager.

qPCR was conducted using the Roche Lightcycler® 480 Instrument with SYBR Green master mix and gene-specific primers (Table S2.1). Primers were optimized by developing standard curves of Ct values of serially diluted cDNA generated from WT *Mtb* H37Rv total RNA. Linear regression modeling was used to calculate amplification efficiencies of qPCR primers for relative quantification of transcripts. Optimal cDNA quantities for RT-qPCR were assessed using serially diluted cDNA and identifying cDNA concentrations with Ct values between 13 and 30 cycles. Each assay included technical replicates, no-reverse transcriptase (NRT) controls, and no

template controls (NTCs). Relative gene expression normalized to *16S rRNA* was determined using the Pffafl method described previously (111). Two-way ANOVA with Tukey's or Šídák's multiple comparisons was performed to determine statistical differences in gene expression between genotypes and conditions (112). All adjusted p-values from the multiple comparisons are listed in Table S2.2.

2.2.4 Resazurin Reduction Assays

Resazurin reduction assays were conducted on defined carbon cultures to indirectly measure metabolic activity. WT and *MtbΔrelE1* cultures were pelleted, washed with 1X TBST, and resuspended in defined carbon conditions at an OD_{600} of 0.05 in 96-well plates. A final concentration of 0.0022mg/mL resazurin sodium salt (Sigma-Aldrich) dissolved in ddH2O was added to *Mtb* cultures seeded at an OD_{600} of 0.05 in 96-well plates. Plates were incubated at 37˚C for 48 hours, and resazurin reduction was detected via absorbance using a Enspire Multimode plate reader at 570 and 600nm. Metabolic activity is represented by percent resazurin reduction normalized to 7H9 or MM, which was calculated using the following formula (113):

$$\frac{(E_{600} * A_{570}) - (E_{570} * A_{600})}{(E_{600} * C_{570}) - (E_{570} * C_{600})}$$

Where:

$E_{570/600}$ = Molar extinction coefficient of oxidized resazurin @ 570/600nm

$A_{570/600}$ = Absorbance of experimental well @ 570/600nm

$C_{570/600}$ = Absorbance of positive control well @ 570/600nm

Significant differences in percent reduction were determined using two-way ANOVA with Šídák's multiple comparisons, with adjusted p-values from pairwise comparisons listed in Table S2.3A.

2.3 Results

2.3.1 *Mtb relBE1* are Encoded in a *Bona Fide* Bi-Cistron

Bacterial genomes often contain polycistrons, or multiple genes that are transcribed into a single mRNA, as an efficient mechanism of gene regulation (114). Additionally, some regulatory genes in *Mtb* have been found to be genomically close to their target genes critical for cell cycle processes (84, 91). The *relBE1* operon is adjacent to *kgd*, which encodes an essential enzyme of the TCA cycle (Figure 2.1).
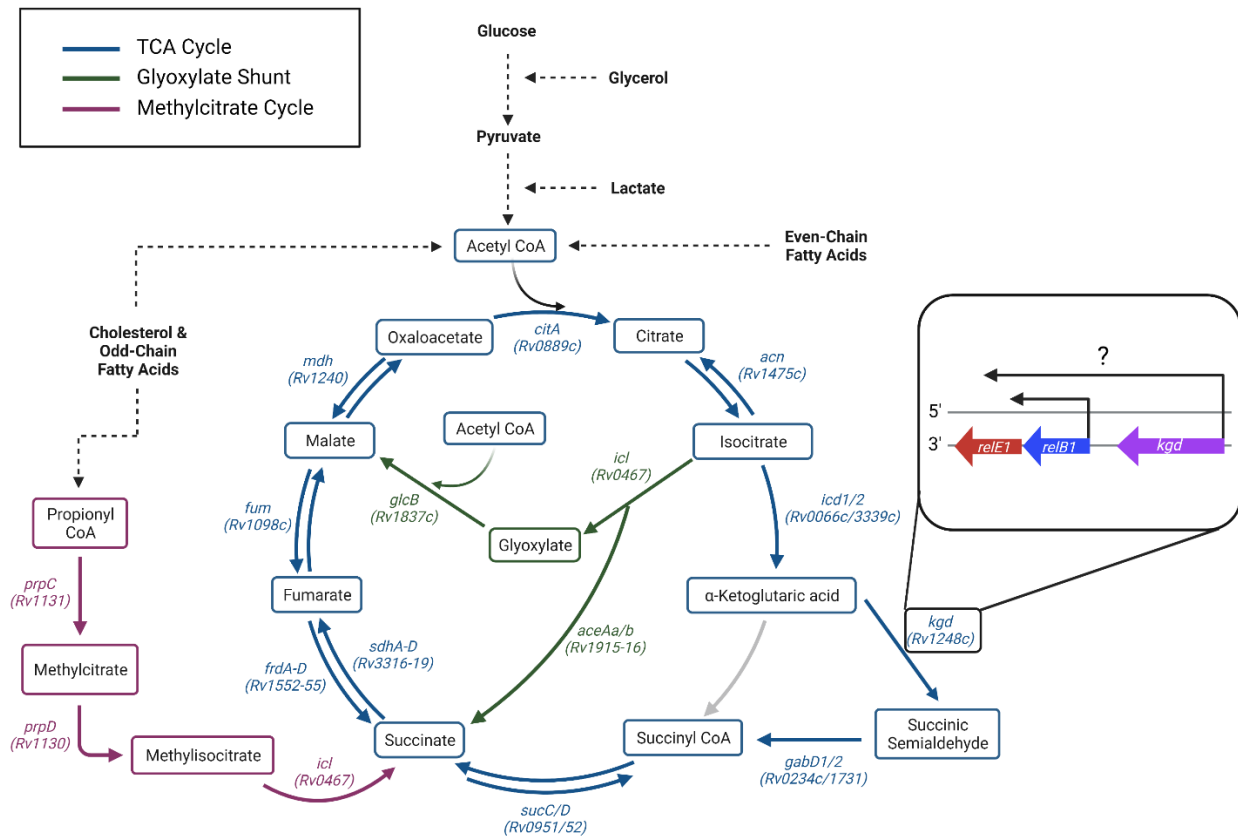
Figure 2.1 *Mtb* TCA cycle schematic with genetic organization of *kgd* in relation to *relBE1*. The metabolic network of *Mtb* outlining the TCA cycle (blue) with the glyoxylate shunt (green) and methylcitrate cycle (purple). Genes that encode metabolic enzymes and their genomic location in *Mtb* are italicized. Dashed arrows represent metabolic pathways of various carbon sources that lead to specific entry points of the TCA cycle. The genomic location of *kgd* relative to *relBE1* is also highlighted on the right. Figure created with Biorender.com.

To assess the potential transcriptional coupling of *relBE1* to central carbon metabolism, we sought to determine if *relBE1-kgd* (*Rv1246c-1248c*) produces a polycistronic transcript. Reverse transcription PCR (RT-PCR) of log-phase *Mtb* H37Rv total RNA was used to analyze *relBE1* and *relBE1-kgd* transcripts. Amplification of *relB1, relE1,* and *kgd,* separately and in combination, from WT *Mtb* cDNA revealed *relBE1* transcripts that support previous findings of the TA system being a bi-cistron (Figure 2.2). However, no transcripts encoding *relBE1-kgd* were detected, suggesting that the genes are not polycistronic.
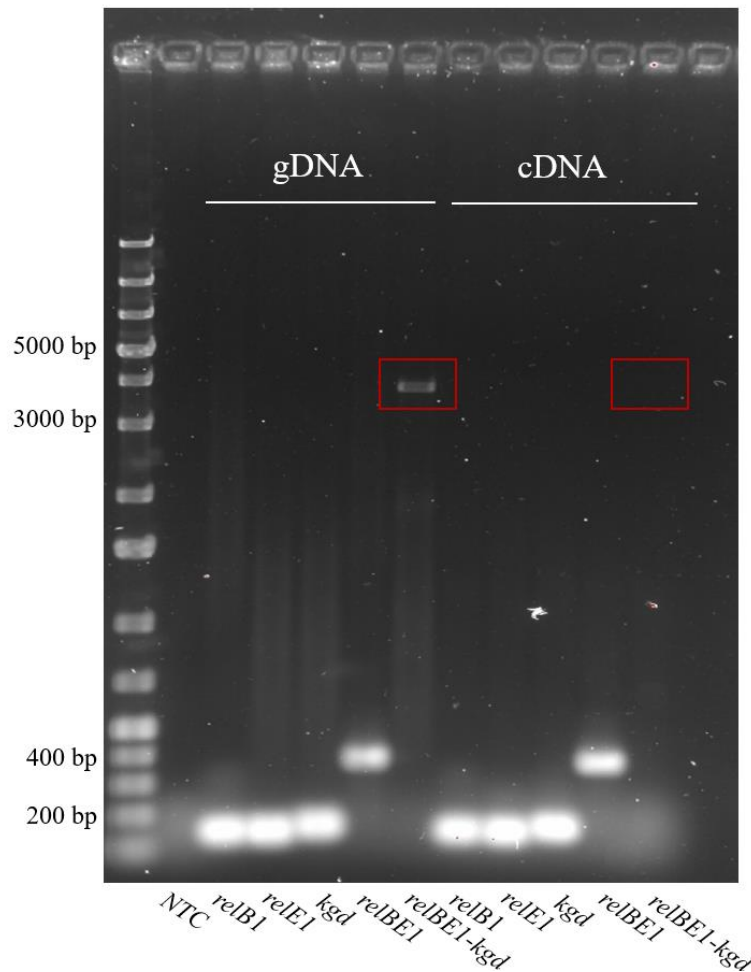
Figure 2.2 RT-PCR of *relB1*, *relE1* and *kgd*. PCR amplification of *relB1, relE1,* and *kgd* from *Mtb* H37Rv complementary DNA (cDNA) generated from 1ug *Mtb* total RNA. *Mtb* gDNA and no template control (NTC) reactions were included for comparison. Amplification of WT *Mtb* H37Rv cDNA was performed using RT-qPCR primers specific to each gene(s) of interest. The red boxes highlight PCR bands representative of *relBE1-kgd* transcripts.

2.3.2 RelE1 is Potentially Required for Glyoxylate Shunt Expression under Cholesterol

Mtb has been extensively shown to undergo metabolic reprogramming under nutrient-limited conditions (47, 96, 100, 102, 103). We sought to test the hypothesis that RelE1 contributes to metabolic adaptation by (1) comparing *relBE1* expression under defined carbon sources and (2) assessing differences in TCA cycle gene expression between WT and *MtbΔrelE1*. WT and mutant strains were grown in minimal media with different carbon sources for up to 24 hours. Relative changes transcript levels of *relB1*, *relE1*, and select genes involved in the TCA cycle (*i.e., icl, kgd, glcB*) were assessed using reverse transcription-quantitative PCR (RT-qPCR). Compared to *Mtb* growth under 7H9, *relE1* expression was found to have a one-to-two-fold decrease under all single carbon sources after one and 24 hours of exposure (Figure 2.3). Growth in the presence of pyruvate and lactate for one hour resulted in an approximately 2-fold increase in *relB1* expression
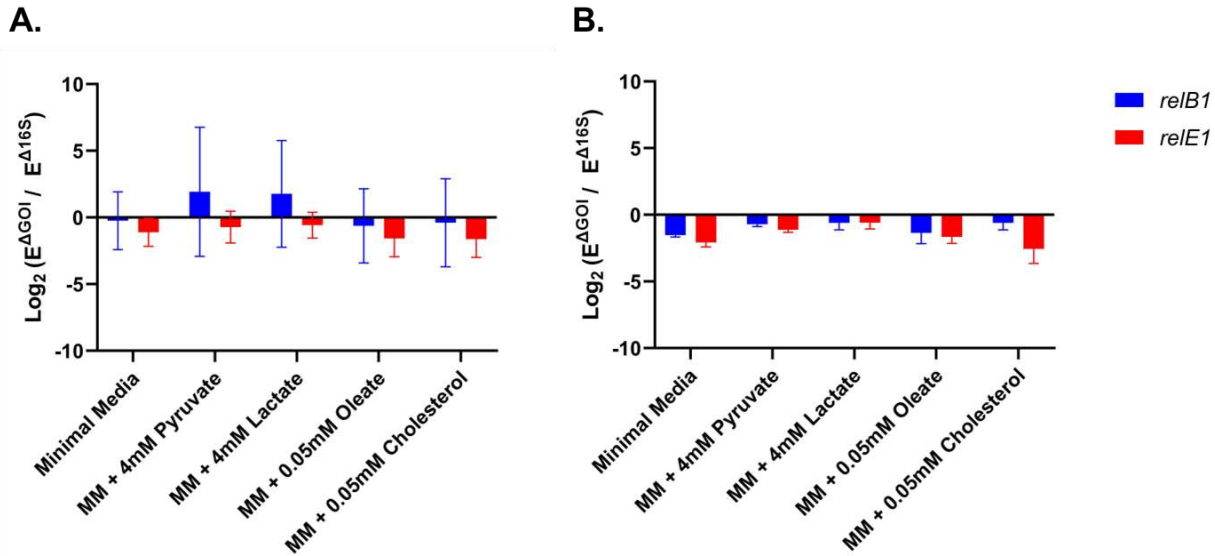
Figure 2.3 *Mtb* H37Rv transcriptional response of *relBE1* under defined carbon conditions. Log-fold expression changes of *relB1* and *relE1* normalized to *16S rRNA* from WT *Mtb* following **(A)** 1-hour and **(B)** 24-hour exposure to single carbon sources relative to growth in 7H9. RT-qPCR data represent log-transformed means and standard deviations of N=2 biological replicates. Significant differences in log-fold expression changes were tested using two-way ANOVA with Tukey's multiple comparisons (Table S2.2A).

(Figure 2.3A). Similar to *relE1*, decreased expression of *relB1* was observed following 24 hours of exposure to all single carbon sources (Figure 2.3B).

We also measured the transcriptional activity of *icl*, *kgd*, and *glcB* from WT and *MtbΔrelE1* in the presence of single carbon sources relative to 7H9 to investigate if *relE1* is required for carbon-mediated shifts in the TCA cycle and glyoxylate shunt (Figure 2.1). The selected genes were chosen because they efficiently capture shifts in carbon flux through the entire TCA cycle versus the glyoxylate shunt under different carbon conditions. Alpha-ketoglutarate decarboxylase converts alpha-ketoglutarate into succinic semi-aldehyde at the lower half of the TCA cycle, moving carbon flow through the entirety of the pathway. The genes encoding isocitrate lyase and malate synthase function within the glyoxylate shunt, which shifts carbon flux away from the bottom portion of the TCA cycle (Figure 2.1).

Overall, no statistically significant differences in the expression of *icl*, *kgd*, and *glcB* were found between WT and *MtbΔrelE1* (Table S2.2B). However, the data showed notable trends in the expression of all three genes under cholesterol conditions (Figure 2.4). The expression of *icl* from WT and *MtbΔrelE1* was comparable to that in 7H9 across all single carbon source conditions except cholesterol (Figure 2.4A). Both genotypes had increased expression of *icl*, but a higher mean log-fold change from WT was observed. WT *Mtb* also presented a slight increase in *kgd* log-fold expression under cholesterol conditions (Figure 2.4B). *ΔrelE1*, on the other hand, presented little to no log-fold change in expression. The expression of *glcB* decreased 2-4-fold across carbon sources, while WT showed a 4-fold increase in expression when in the presence of cholesterol (Figure 2.4C). Together with *relBE* expression data, these findings suggest RelE1 may be required for cholesterol-mediated expression of *icl* and *glcB* despite the lack of transcriptional activity of *relE* following 24 hours of exposure.
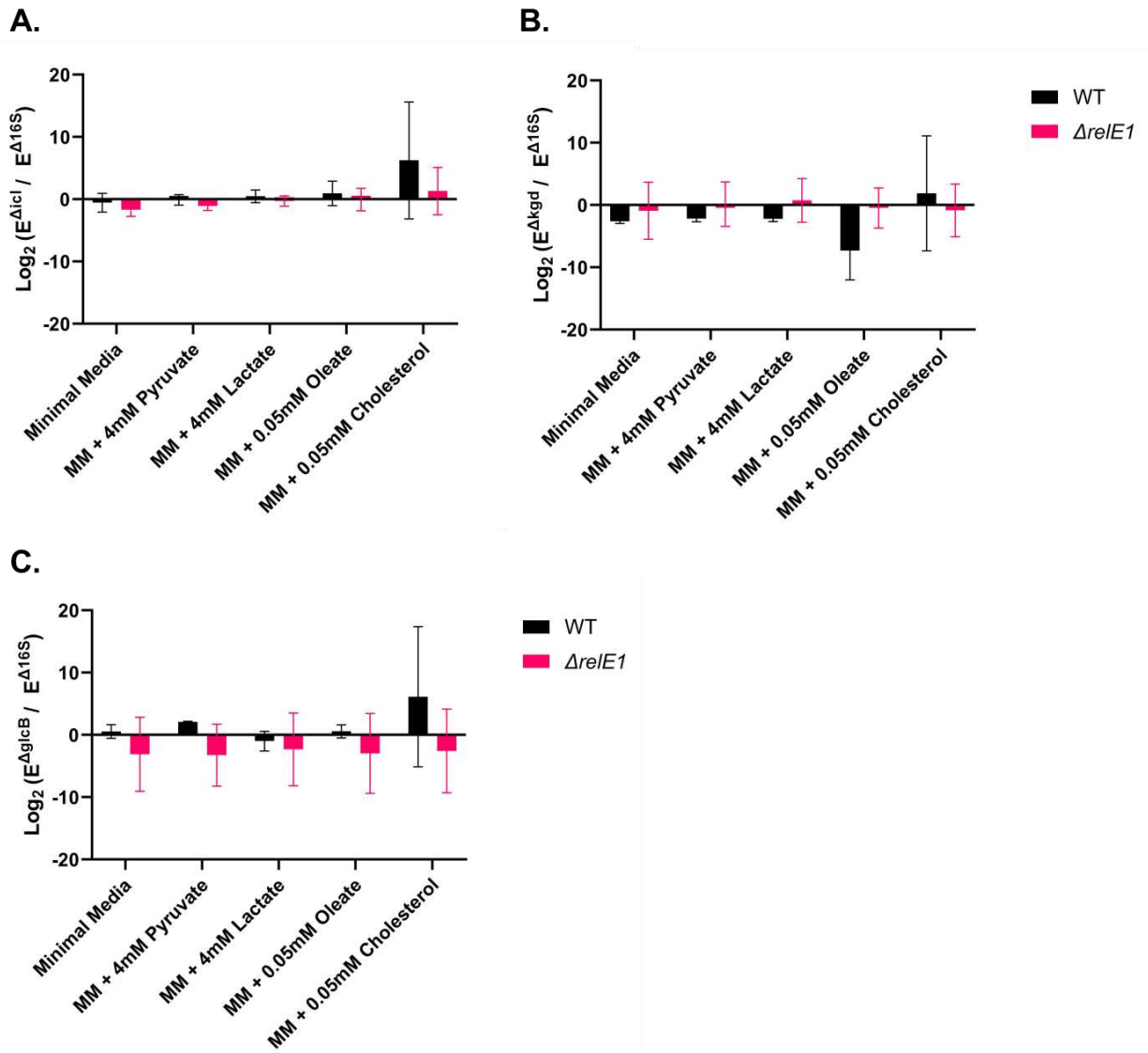
Figure 2.4 Differences in TCA cycle transcriptional responses between WT and *MtbΔrelE1*. Log-fold expression changes **of (A)** *kgd,* **(B)** *icl,* and **(C)** *glcB* normalized to *16S rRNA* from WT and *MtbΔrelE1* following 24-hour growth in single carbon sources relative to that in 7H9. RT-qPCR data represent log-transformed means and standard deviations of N=2 biological replicates. Significant differences in log-fold expression changes were tested using two-way ANOVA with Šídák's multiple comparisons (Table S2.2B).

2.3.3 RelE1 Likely Contributes to Metabolic Adaptation under Lipid and Nutrient Starvation Conditions

Lipids, especially cholesterol, are abundant in the granuloma microenvironment during infection, and *Mtb* likely relies on lipids as major carbon sources for survival (37, 57, 106,

107). We aimed to investigate the requirement of RelE1 in *Mtb* survival under oleate, an even-chain fatty acid, and cholesterol. We also assessed survival under pyruvate and lactate, glycolytic products of glucose or glycerol, that feed into the TCA cycle for comparison. Some previous literature explored *Mtb* metabolism and metabolic flux using 7H9 as a base medium, in which more than one carbon source is present. Other studies used minimal medium (MM), where the only carbon source available is one that is supplemented to the base medium.

Here we compared both methods for a more thorough analysis of *Mtb* response to different carbon sources. 7H9-based conditions will be defined as supplemented or supplemented carbon sources, and conditions based in MM will be referred to as single carbon source conditions. Metabolic activity of WT and *MtbΔrelE1* in the presence of single or supplemented carbon sources was measured after 48 hours, and bacterial growth and viability were assessed over the course of six days. Metabolic activity of *Mtb* H37Rv was determined using resazurin, a compound that is reduced to resorufin by metabolically active cells via aerobic respiration (Figure 2.5).
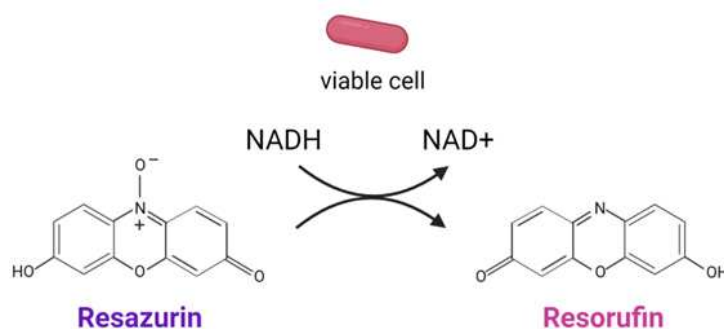
Figure 2.5 Reduction of resazurin by metabolically active cells. Resazurin is often used to measure metabolic activity of cells. Incubation of resazurin with respiring cells results in the NADH-dependent reduction of the purple resazurin substrate to a pink resorufin product. Figure created with Biorender.com.

Mtb possessed consistent metabolic responses amongst carbon sources supplemented in 7H9 (Figure 2.6A). Exposure to supplemented oleate and cholesterol resulted in a slight reduction

of metabolic activity from *ΔrelE1* compared to WT, indicating a possible contribution of RelE1 in optimal *Mtb* metabolism under supplemented lipids. Growth under 1X TBST presented a statistically significant difference in percent resazurin reduction between WT and *ΔrelE1*, which suggests that RelE1 toxins are required for *Mtb* metabolic adaptation in nutrient starvation conditions (Figure 2.6A, Table S2.3A). WT and *ΔrelE1* both exhibited reduced metabolic activity under oleate and cholesterol as single carbon sources compared to carbohydrates and glycolytic carbon sources (Figure 2.6B). However, no significant differences in percent reduction were observed between WT and *ΔrelE1*.
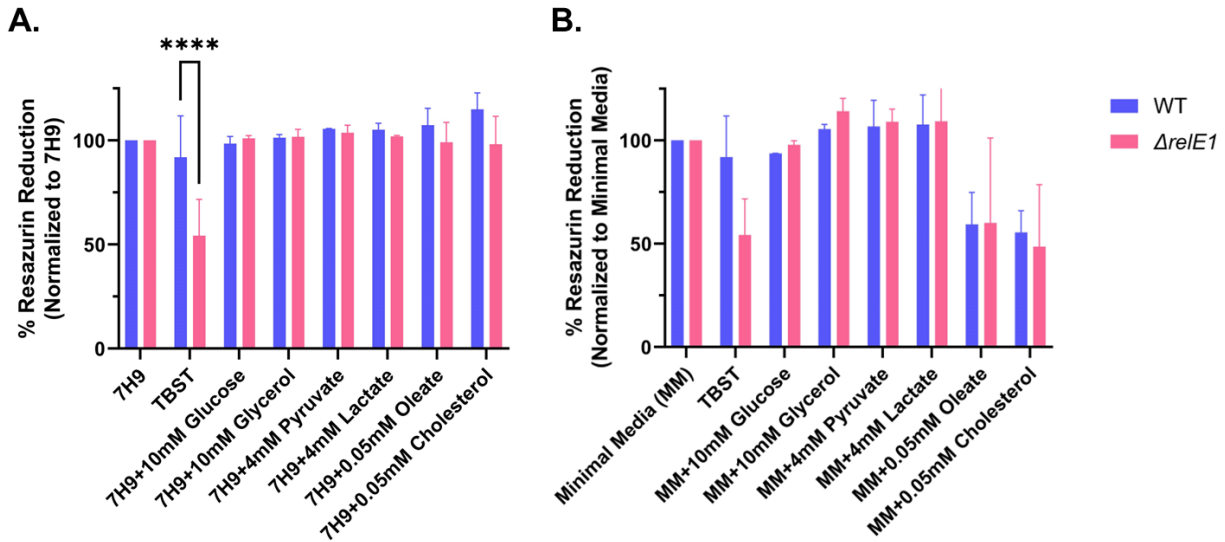
Figure 2.6 *Mtb* H37Rv metabolic activity under different carbon sources. WT and *MtbΔrelE1* normalized percent resazurin reduction following exposure to **(A)** supplemented carbon and **(B)** single carbon sources. Cultures were seeded at OD_{600} = 0.05 with a final concentration of 0.0022mg/mL resazurin. Absorbances at 570 and 600nm were recorded following incubation at 37°C for 48 hours, and percent reduction normalized to 7H9 or MM was calculated for each sample. Data represent means and standard deviations of N=3 biological replicates, except for 10mM glucose and 10mM glycerol (N=2). Significance between genotypes was assessed using two-way ANOVA with Šídák's multiple comparisons (****$p < 0.0001$, Table S2.3A).

Given that (1) resazurin reduction was similar between glucose/glycerol and pyruvate/lactate growth conditions (Figure 2.6) and (2) pyruvate and lactate are the products of

glucose and glycerol catabolism, we only incorporated pyruvate, lactate, oleate, and cholesterol in growth and outgrowth experiments. WT *Mtb* growth and survival under supplemented lipid verses glycolytic carbon sources after six days were overall comparable to 7H9 alone (Figure 2.7A, B). *Mtb* grew slightly better in supplemented pyruvate and lactate, but no differences in growth nor Log_{10} CFU/mL were found between WT and *ΔrelE1* (Figure 2.7A). Interestingly, *ΔrelE1* exhibited diminished growth under 0.05mM lipids after 48 hours compared to WT (Figure 2.7B). Growth under oleate and cholesterol after six days was reduced in *ΔrelE1* compared to WT, with the difference being statistically significant under oleate (Figure 2.7B, Table S2.3B). However, no differences in Log_{10} CFU/mL between genotypes in supplemented lipids were observed after six days of exposure (Table S2.3B). Despite the decrease in OD_{600} over the course of six days, Log_{10} CFU/mL of both strains in TBST suggest that nutrient starvation induces non-replicative persistence (Figure 2.7A, B).
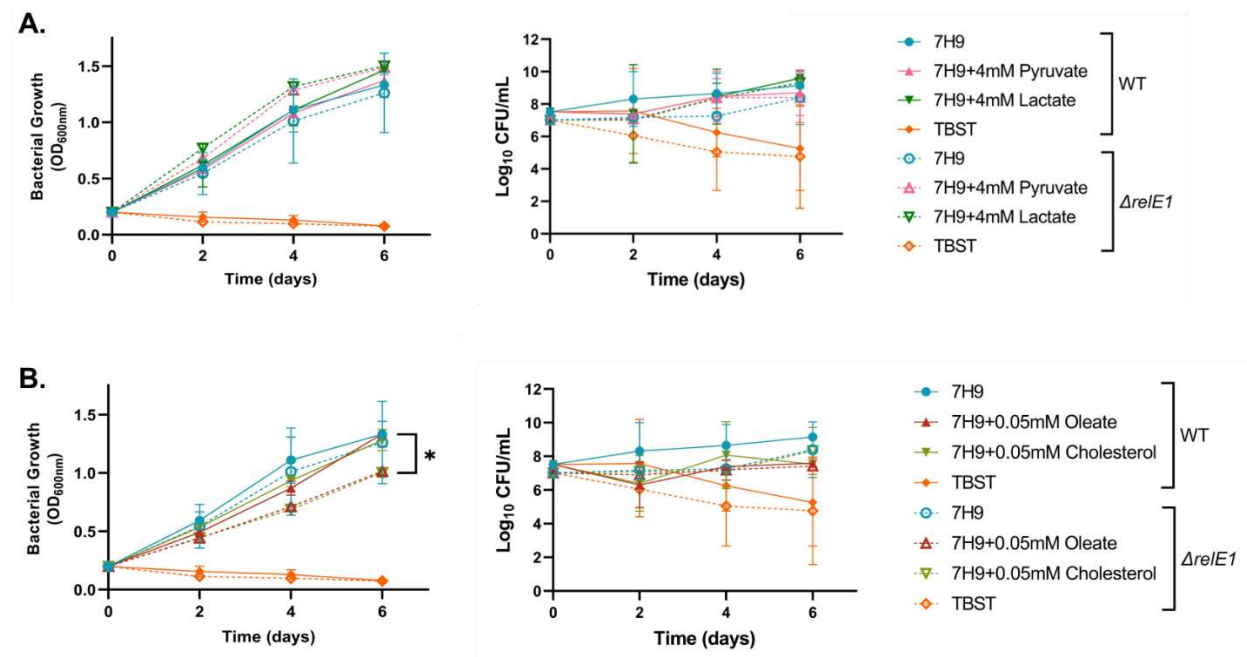
Figure 2.7 *Mtb* H37Rv growth and survival under supplemented carbon sources. WT and *MtbΔrelE1* growth (left panel) and outgrowth (right panel) under **(A)** 4mM pyruvate or lactate and **(B)** 0.05mM oleate or cholesterol supplemented in 7H9. Cultures were seeded at $OD_{600} = 0.2$.

OD_{600} recordings were taken and CFUs were enumerated every 48 hours. Data depict the means and standard deviations of N=2 biological replicates. Significant differences in growth between WT and *ΔrelE1* were calculated using mixed model ANOVA with Tukey's multiple comparisons (*$p < 0.05$, Table S2.3B, C).

Unlike supplemented carbon conditions, no increase in biomass was observed following exposure to single carbon sources (Figure 2.8A, B). Log_{10} CFU/mL for both strains in the presence of single carbon sources showed no significant decrease in survival over six days, which indicated that *Mtb* establishes non-replicative persistence under single carbon source conditions. *ΔrelE1* appeared to have slightly increased growth relative to WT in the presence of pyruvate and lactate but with minor reductions in Log_{10} CFU/mL (Figure 2.8A, B). In the span of six days, no differences were discerned between the two genotypes following exposure to oleate nor cholesterol (Figure 2.7B). *Mtb* growth under the lipid conditions are comparable to that of 1X TBST, but Log_{10} CFU/mL of *MtbΔrelE1* in the presence of oleate was slightly higher than that of WT.
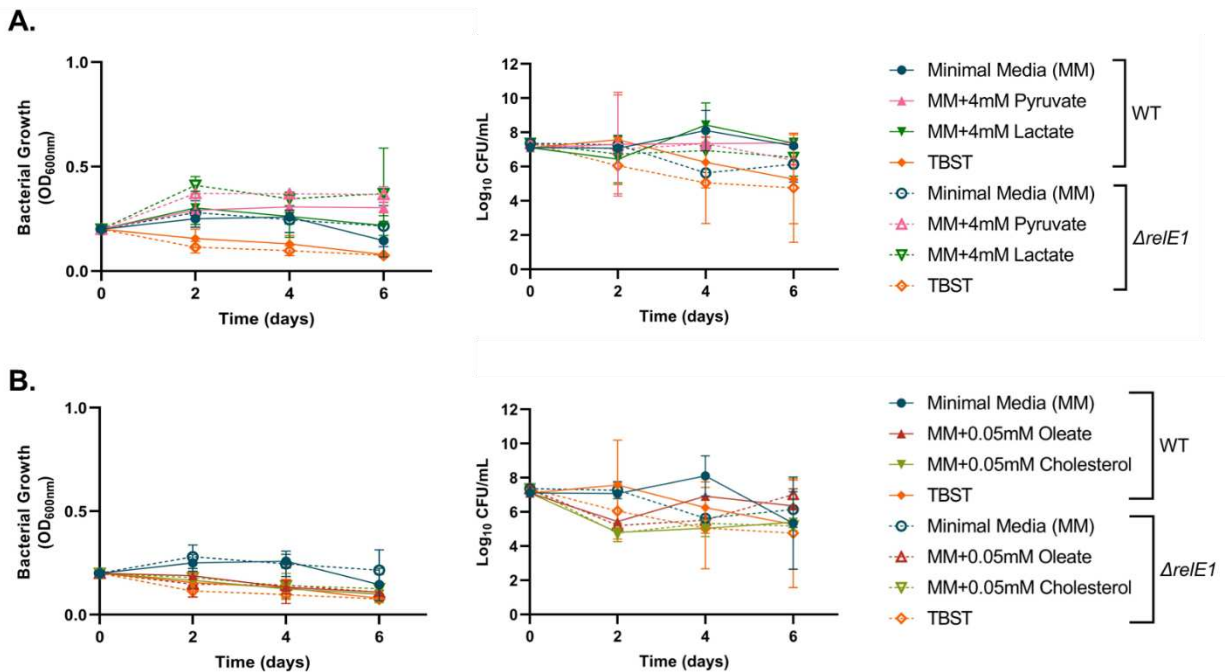
Figure 2.8 *Mtb* H37Rv growth and survival under single carbon sources. WT and *MtbΔrelE1* growth under **(A)** 4mM pyruvate or lactate and **(B)** 0.05mM oleate or cholesterol supplemented in minimal media. Cultures were seeded at $OD_{600} = 0.2$. OD_{600} recordings were taken and CFUs were

enumerated every 48 hours. Data are representative of the means and standard deviations of N=2 biological replicates. Statistical differences between genotypes were assessed using mixed model ANOVA with Tukey's multiple comparisons (Table S2.3 B, C).

2.4 Discussion

This study aimed to investigate the impact of the RelBE1 TA system in *Mtb* adaptation to defined carbon conditions. We first sought to assess potential transcriptional coupling of *relBE1* to central carbon metabolism via polycistronicity between the TA locus and the target metabolic gene, *kgd*. RT-PCR data of *relBE1* and *kgd* do not implicate transcriptional coupling between the TA locus and metabolic gene, but we did confirm that *relBE1* is a bona-fide bi-cistron. (Figure 2.2). It is worth noting that RelBE1 could indirectly regulate *kgd* by cleaving mRNAs that, in turn, directly or indirectly influence *kgd* expression. The TA system may also regulate other members of central carbon metabolism in the response of *Mtb* to host-induced stresses. Future studies could be designed to better identify targets of *relBE1*-mediated regulation at the transcriptional or translational levels.

Additionally, we determined the transcriptional responses of *relBE1* under defined carbon conditions. No relative transcriptional activity was observed for *relE1* under different single carbon sources. However, *relB1* increased in expression after 1 hour of exposure to pyruvate and lactate (Figure 2.2). This could be explained by the induction of the operon following the degradation of RelB1 proteins, which would indicate the presence of free RelE1 proteins that were not detected on a transcriptional level at the tested timepoints (74, 115). Some experts in the field of TA systems argue that transcriptional activity is not the best indicator of biological activity and toxin and antitoxin protein levels would stand as stronger evidence for physiological impact on processes like stress response or persister cell formation (80). Future work on *Mtb* TA systems

34

should incorporate targeted proteomics in conjunction with transcriptional data to make direct links between TA system function and *Mtb* pathogenesis.

The analysis of WT versus *MtbΔrelE1* TCA cycle gene expression under single carbon source conditions revealed differences following 24 hours of exposure to cholesterol that suggest a potential connection between RelE1 and TCA cycle flux towards the glyoxylate shunts in the presence of cholesterol (Figure 2.3). The expression data presented a moderate level of variability, so the confidence in these trends being biologically accurate is unfortunately low. However, raising the statistical power by increasing the number of replicates would help to discern differences in log-fold changes in expression.

When assessing *Mtb* growth, metabolic activity, and overall survival under nutrient-rich conditions, we found evidence suggesting that RelE1 might be required for optimal growth in supplemented lipids as indicated by the differences in OD_{600} and metabolic activity between WT and *MtbΔrelE1* (Figures 2.6A, 2.7B). However, no variation in Log_{10} CFU/mL was detected to indicate RelE1 being required for the survival of *Mtb* under these conditions. No changes in *Mtb* viability following exposure can be attributed to the presence of other carbon sources in the 7H9 base medium. The low statistical power of the experiments acts as a notable limitation in these studies; increasing the number biological replicates would likely provide more statistically significant evidence of RelE1 being required for metabolic adaptation and, subsequently, optimal growth when exposed to cholesterol or oleate. Given the transcriptional trends under these two conditions, it can be speculated that RelE1 acts on pathways and mechanisms within the TCA cycle and glyoxylate shunt for the regulation of cholesterol metabolism and growth but likely outside the tested metabolic pathways when regulating that in the presence of oleate.

With single carbon conditions, we did not find evidence supporting our hypothesis that RelE1 is required for *Mtb* survival in lipid conditions. However, *Mtb* appears to undergo non-replicative persistence in the presence of single carbon sources regardless of the carbon type (Figures 2.6B, 2.8A, B). Growth over the course of six days did not increase, but metabolic activity and viability were detected under these conditions. Interestingly, *MtbΔrelE1* growth under pyruvate and lactate was slightly greater than that under minimal media alone, while oleate and cholesterol conditions resulted in relatively lower OD_{600} (Figure 2.8A, B). *MtbΔrelE1* metabolism was notably reduced in the presence of oleate and cholesterol as single carbon sources, but sustained Log_{10} CFU/mL under these conditions provides evidence of viability over time (Figure 2.6B, 2.8B). These trends are indicative of how *Mtb* likely responds to nutrient limitation during infection.

Interestingly, we found that WT and *MtbΔrelE1* had significantly different metabolic activities under TBST conditions, which acted as a negative growth control (Figure 2.6A, B). 1X TBST consists of tris-buffered saline with 0.1% Tween 80, a surfactant used to prevent clumping of tubercle bacilli in liquid cultures and contains no significant source of carbon. Given the viability of *Mtb* in TBST after six days (Figures 2.7, 2.8), our findings suggest that RelE1 is required for metabolic adaptation and survival when *Mtb* experiences nutrient starvation. It is thought that *Mtb* exhibits nutrient deprivation during infection, and mycobacteria have been shown to tolerate drug exposure under *in vitro* starvation models (46, 116). Alternatively, Tween 80 could present toxicity to *Mtb* that is mediated by functional RelE1. Further studies assessing the relationship between RelBE1 and *Mtb* adaptation under TBST would be needed to confirm and strengthen the confidence of our findings.

Metabolic adaptation to various stress conditions is required for the survival of *Mtb* and overall success as a pathogen. The work presented here dissected *in vitro Mtb* responses to a range of carbon sources and found that the RelBE1 TA system is required for the adaptation and survival to nutrient starvation and possibly involved in optimal growth and metabolism under supplemented oleate and cholesterol.

CHAPTER 3: CRISPRI-MEDIATED GENE SILENCING OF *RELBE* TA SYSTEMS AS A TOOL TO DISSECT TA SYSTEM FUNCTION IN *MYCOBACTERIUM TUBERCULOSIS*

3.1 Introduction

The global burden of TB has been a significant challenge to manage due to the large number of latent infections that often go undetected. *M. tuberculosis* possesses the ability to establish latent infections by lying dormant in its host for up to decades before initiating an active infection. Throughout infection, *Mtb* encounters environments established by the host immune response in an attempt to clear the infection, which can include low-pH, hypoxia, and nutrient limitation (39). For *Mtb* to survive the harsh microenvironment of its host, the pathogen must have strict control over its metabolic networks. Decades of research have demonstrated that *Mtb* alters its metabolism and replication rate in response to stress (53, 56, 117, 118). *Mtb* has been shown to rely on specific metabolic pathways and their components to survive host immune responses, tolerate antibiotic exposure, and disrupt host cellular processes (56, 119, 51, 52, 57, 60, 47, 54, 120, 96, 121, 122, 100). For instance, Pandey and others found that *Mtb* requires host cholesterol for long-term persistence during chronic infection and identified a gene cluster that encodes factors that control the import of cholesterol (57). Further investigation revealed distinct changes in *Mtb* metabolism following cholesterol exposure, including the induction of genes involved in the methylcitrate cycle required for the catabolism of propionyl-CoA (47).

The regulatory networks underpinning metabolic reprogramming at different stages of TB disease have been explored, but there are still significant gaps in our understanding of metabolic regulation (54, 56, 63, 83, 123). *Mtb* harbors a surprising number of toxin-antitoxin (TA) systems that have been implicated in pathogenesis (83, 81, 124–127), but we have yet to fully define the

relationship between these regulatory elements and the underlying mechanisms of persistence during infection (70, 78, 80, 128). Dissecting the physiological functions of TA systems in *Mtb* is particularly challenging due to the vast number of TA loci. A growing number of studies argue against the relationship between TA systems and stress response, claiming that evidence supporting the hypothesis is weak and inconsistent (80, 128, 70, 79). Previous work has attempted to identify the biological relevance of specific TA systems in *Mtb*, but no studies to date have been able to fully elucidate the cooperative function of all TA systems in *Mtb* persistence, survival, or virulence using robust genetic controls (83, 84, 87, 129). TA systems stand as promising targets for novel therapeutics against latent infections, but we need to first understand the precise physiological roles they play in *Mtb* pathogenesis.

Mtb is a slow-growing pathogen, which makes genetic manipulation especially time-consuming. Generating a single knockout can take months to complete using traditional cloning methods; producing *Mtb* strains with multiple knockouts significantly extends the required time and resources (130–132). When dissecting numerous TA systems and their potential roles in *Mtb* pathogenesis, it is logical to apply genetic manipulation to all TA loci within a given family. The rise and advancement of CRISPR technologies have made it feasible to manipulate individual and multiple genes within a single system (131, 133). This work incorporates a CRISPR-interference (CRISPRi) system developed by the Fortune Lab (131). Using an inactivated Cas9 (dCas9) enzyme from *Streptococcus thermophilus* and short-guide RNAs (sgRNAs), this system physically blocks the transcription of targeted genes in mycobacteria. As illustrated in Figure 3.1, the *S. thermophilus* dCas9 protein interacts with the sgRNA, and the complex binds to the target DNA. The sgRNA incorporates the targeted DNA sequence and thus guides dCas9 to the sequence of interest. The complex can successfully bind to the DNA when dCas9 recognizes a protospacer

adjacent motifs (PAM) in the sequence near the targeted region (NGGNG). This system specifically includes Golden Gate cloning sites that enable efficient and inducible silencing of multiple genes at once (131).

We sought to apply this system towards developing a molecular tool for assessing multiple TA systems in *Mtb*. As a proof of concept, we aimed to (1) silence the expression of three *relBE* TA systems in *Mtb* and (2) assess the metabolic activity of the knockdown mutants under defined carbon conditions to further investigate the physiological function of RelBE TA systems in *Mtb* carbon-mediated adaptation. The development of this molecular tool allows for more robust studies of gene function in *Mtb* and helps dissect potential functional redundancies of TA systems, which is critical to expand our understanding of *Mtb* persistence during infection.

3.2 Materials and Methods

3.2.1 Bacterial Strains and Experimental Growth Conditions

M. tuberculosis H37Rv and *E. coli* DH5-α strains were used in the present study. *Mtb* liquid cultures were maintained in 7H9 Middlebrook medium supplemented with 10% OADC and 0.05% Tyloxapol (Tylox, Sigma-Aldrich) and incubated at 37°C with constant shaking at 200rpm. *E. coli* cultures were grown in LB medium at 37°C, 200rpm. Where indicated, antibiotics (Sigma Aldrich) and derivatives (Takara Bio USA) were used at the following concentrations: kanamycin (Kan, 25µg/mL and 50 µg/mL) for *Mtb* and *E. coli*, respectively, and anhydrotetracycline (ATc, 100ng/mL) for both *Mtb* and *E. coli*.

3.2.2 Cloning and *Mtb* Mutant Generation

All constructs generated in the study are listed in Table S3. Cloning was achieved using the protocol published by Andrew Wong and Jeremy Rock (134). The CRISPRi knockdown

mutant that simultaneously targets *relBE1*, *relBE2*, and *relBE3* was generated using sgRNAs designed to target the open reading frame (ORF) on the non-template strand of each bi-cistron with an effective PAM sequence located on the template strand (Table S3.1). Work by Rock *et al.* identified viable PAM sequences that are recognized by *S. thermophilus* dCas9, and PAM sequences with greater than 25-fold repression were chosen when designing sgRNAs for each target (131). Each sgRNA oligo was annealed with its respective reverse complement sequence to generate a double-stranded sequence compatible with the BsmBI-digested backbone, PLJR965 (Addgene Plasmid #115163, 135). All individual sgRNAs were cloned into PLJR965 to generate single knockdown mutants, and SapI Golden Gate cloning was performed to ligate all promoter-sgRNA-terminator cassettes with the parent vector. Each cassette was amplified using primers with SapI-restriction sites and overhang sequences compatible with the Golden Gate handle in the backbone (Table S3.1). Transformations of final constructs into *E. coli* DH5-α were performed based on manufacturer instructions, and transformed constructs were verified using diagnostic restriction digestion and Sanger sequencing.

Verified constructs were transformed into *Mtb* H37Rv as described previously (135). Briefly, mid-log *Mtb* cultures were supplemented with 0.1 volumes 2 M glycine 24 hours before harvesting. Cultures were then pelleted at 3,500rpm, 4°C for 10 minutes and washed three times with 10% glycerol at RT, decreasing the volume of glycerol used with each subsequent wash. Cells were resuspended in 10% glycerol, and 0.2-mL aliquots were used for electroporation. Fresh electrocompetent cells were combined with 5uL of 100-200ng DNA and transferred to 2mm-gap cuvettes. Samples were electroporated at 2.5 kV, 25 µF, 1000Ω using the BioRad Micropulser. Electroporated cells were immediately transferred to 10mL 7H9 broth without selection and

incubated at 37 ˚C, shaking for 24 hours. Cultures were harvested by centrifugation, plated onto selective 7H10 plates, and incubated for 21 to 28 days until colonies formed.

3.2.3 Relative Quantification of *relBE* Silencing

To assess the silencing efficiency of *relBE1*, *-2*, and *-3* by CRISPRi, mutant cultures were induced with 100ng/mL anhydrotetracycline (ATc) for 24 to 72 hours. Briefly, mid-log cultures of each mutant were diluted to an OD_{600} of 0.2 and split into induced and non-induced groups. ATc-induced cultures were transferred to light-protective 50-mL conical tubes to prevent degradation of ATc over time. All subcultures were incubated at 37 ˚C, shaking at 200rpm. Every 24 hours, 25mL of each culture was pelleted, washed with 1X TBST, and resuspended in 1mL TRIZol Reagent (Invitrogen). Cells were mechanically lysed as described in Chapter 2 for subsequent RNA extraction and qRT-PCR.

Total RNA was extracted as described in Chapter 2, and cDNA was generated from 1µg DNase-treated RNA and random hexamer primers using the FirstStrand cDNA Synthesis kit (Roche). qPCR was conducted on cDNA from uninduced and ATc-induced samples, and each assay included technical replicates, NRT controls, and NTCs. Log-fold gene expression changes normalized to *16S rRNA* were determined using the Pffafl method (111). Two-way ANOVA with Tukey's multiple comparisons was performed to determine statistical differences in gene expression. Adjusted p-values are listed in Supplementary Table S3.2.

3.2.4 Resazurin Reduction Assays of Induced CRISPRi Mutants

Single- and combined- knockdown mutants were subjected to defined carbon conditions, and metabolic activity was assessed via resazurin reduction assays. Briefly, mid-to-late log cultures were pelleted, washed once with 1X TBST, and resuspended in either carbon-

supplemented 7H9 or minimal medium (MM). A final concentration of 0.0022mg/mL resazurin sodium salt (Sigma-Aldrich) dissolved in ddH2O was added to mutant cultures seeded at an OD_{600} of 0.05 in 96-well plates. Plates were incubated at 37°C, and resazurin reduction was detected after 72 hours via absorbance using a Enspire Multimode plate reader at 570 and 600nm. Metabolic activity is represented by percent resazurin reduction normalized to 7H9 or minimal media. Significant differences in percent reduction between each mutant and WT *Mtb* were determined using two-way ANOVA with Dunnett's multiple comparisons, with adjusted p-values from pairwise comparisons listed in Table S3.3.

3.3 Results

3.3.1 CRISPRi Mutants Produce Variable Silencing Efficiencies Following ATc Induction

While *Mtb* harbors numerous TA systems with similar biochemical activities, previous work has only focused on the identification and biological relevance of individual TA loci. To more effectively address the potential functional redundancy or cooperativity of RelBE TA systems in *Mtb*, we sought to silence *relBE1, -2,* and *-3* simultaneously using CRISPRi (Figure 3.1). The sgRNA for each individual *relBE* bi-cistron was designed to target the ORF of the *relB* gene and utilizing the polar effect of CRISPRi to additionally silence the adjacent *relE* gene (132). The polar effect of CRISPRi is observed because the sgRNA-dCas9 complex physically blocks RNA Polymerase from transcribing the target gene and thus any gene downstream of the target. While this phenomenon is usually seen as a significant limitation of CRISPRi, this application takes advantage of this silencing effect. The three sgRNAs were then combined into a single vector using Golden Gate cloning for the simultaneous repression of *relBE* transcription.
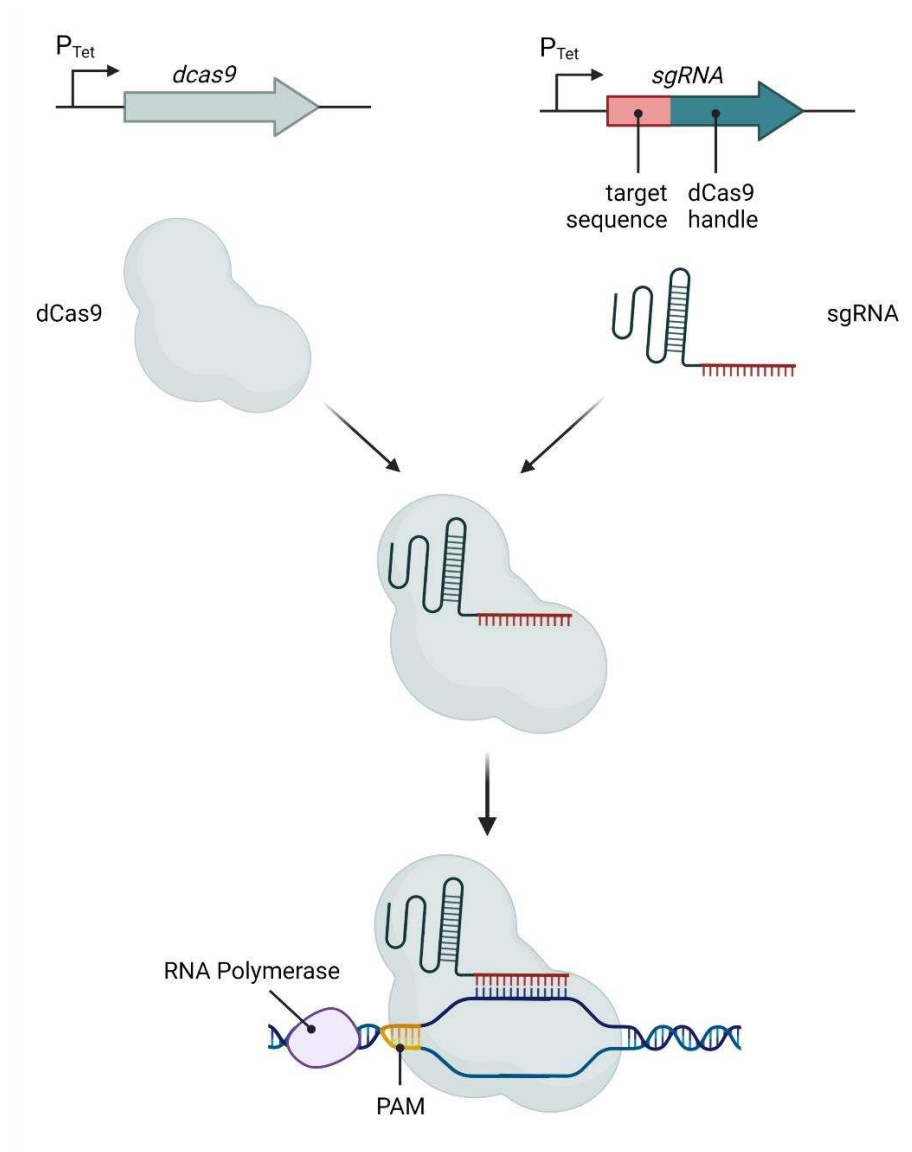
Figure 3.1 CRISPRi mechanism for targeted gene silencing. Schematic of anhydrotetracycline (ATc)-inducible transcriptional repression of target genes. The deactivated Cas9 (dCas9) and short-guide RNA (sgRNA) interact with one another, bind to target DNA, and physically block RNA polymerase from transcribing the targeted DNA sequence. The protospacer adjacent motif (PAM) is located near the target sequence for dCas9 recognition. Figure created with Biorender.com.

Mtb H37Rv transformed with individual and combined knockdown constructs showed varied success of transcriptional repression following ATc induction (Figure 3.2A-D). Compared to the no-induction control, *PLJR-relBE1* exhibited significant silencing of both *relB1* and *relE1* after 72 hours (Figure 3.2A, Table S3.3). *PLJR-relBE2* did not effectively silence *relB2* nor *relE2*,

and *PLJR-relBE3* only presented a minor silencing effect of *relBE3* after 72 hours of ATc induction (Figures 3.2B, C). For unknown reasons, induction with ATc resulted in increased expression of the targeted *relBE2* and *relBE3* operons. The construct pertaining to all three *relBE* operons produced a silencing effect of each gene after 72 hours of ATc induction, but the silencing efficiencies vary and are not statistically significant relative to the uninduced control (Figure 3.2D). These data suggest that *relBE1, -2,* and *-3* can be transcriptionally repressed under a single CRISPRi system with three days of ATc induction, but with variable efficiencies. It is important to note that this assessment involved only one biological replicate, so RT-qPCR should be performed on additional replicates in order to confirm our findings. Additionally, the transcriptional activity does not directly indicate the prevalence of RelBE proteins present before and after ATc induction.
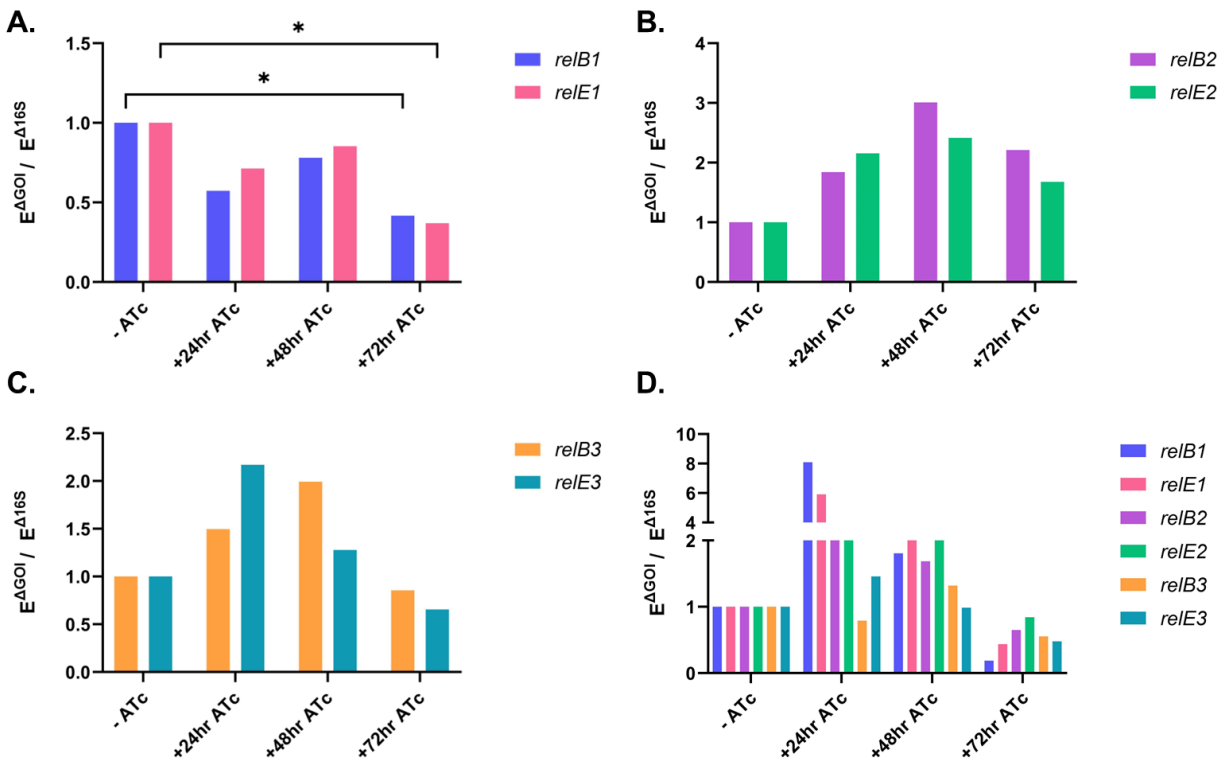
Figure 3.2 *Mtb* transcriptional responses of *relBE* following ATc induction. Relative expression of *relB* and *relE* genes normalized to *16S rRNA* from *Mtb* (**A**) *PLJR-relBE1*, (**B**) *PLJR-relBE2*, (**C**) *PLJR-relBE3*, and (**D**) *PLJR-relBE1-3* following 24-72 hours of ATc induction. RT-qPCR data represent N=1 experiment. Significant differences in relative expression were determined using two-way ANOVA with Tukey's multiple comparisons (*$p < 0.05$; Table S3.3).

3.3.2 *Mtb* Exhibits Differential Metabolic Responses to Defined Carbon Conditions Following Silencing Of *relBE* TA Systems

To investigate the potential cooperation or duplicated function of multiple RelBE TA systems in *Mtb*, we applied the CRISPRi constructs under defined carbon conditions and assessed potential changes in *Mtb* metabolic responses compared to WT and *ΔrelE1* strains. Individual and combined knockdown strains were induced and exposed to defined carbon conditions tested in Chapter 2, consisting of 7H9 or minimal medium (MM) supplemented with different carbon sources. Metabolic activity via resazurin reduction was detected after 72 hours of carbon exposure since ATc induction produced the best silencing efficiencies at 72 hours (Figure 3.2).

Mtb mutants showed close to 100% resazurin reduction in all supplemented carbon conditions, with 1X TBST producing roughly 50% reduction across all strains (Figure 3.3A). Compared to WT *Mtb*, each CRISPRi knockdown presented a significant decrease in metabolic activity under TBST. Additionally, the difference in resazurin reduction between WT and *PLJR-relBE1* under supplemented cholesterol was statistically significant (Figure 3.3A, Table S3.4A). Single carbon sources differed from supplemented carbon conditions and resulted differential metabolic responses between the induced mutants and WT. Metabolic activity in the presence of carbohydrate-based carbon sources across genotypes was comparable to that under minimal media alone, while only about 50% activity following exposure to lipid carbon sources across genotypes was observed (Figure 3.3B). Even though evidence of RelBE functional redundancy or

46

cooperativity was not found, these data successfully demonstrate the application of CRISPRi to dissect physiological function of multiple genes in *Mtb*.
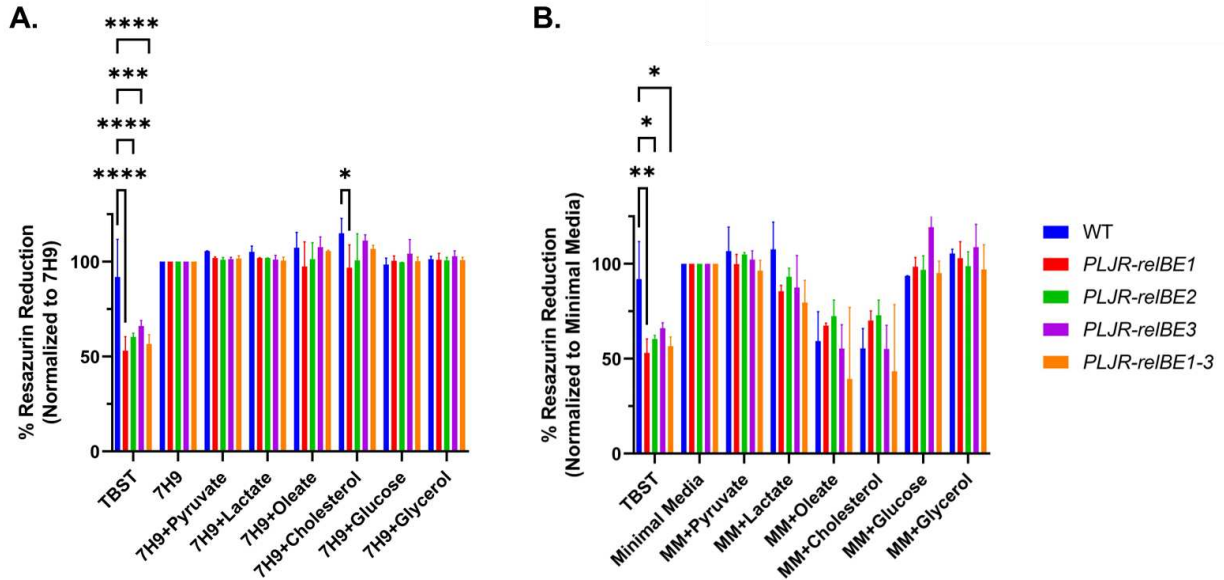
Figure 3.3. Metabolic activity of induced *Mtb* CRISPRi mutants. Percent resazurin reduction of *Mtb* H37Rv *relBE* ATc-induced knockdown mutants following exposure to **(A)** supplemented carbon and **(B)** single carbon sources. Cultures were seeded at $OD_{600} = 0.05$ with 0.11mg/mL resazurin for a final concentration of 0.0022mg/mL. Absorbances at 570 and 600nm were recorded following incubation at 37˚C for 72 hours, and percent reduction normalized to 7H9 or MM was calculated for each sample. Data represent means and standard deviations of N=2 biological replicates. Significance between genotypes was assessed using two-way ANOVA with Dunnett's multiple comparisons (*$p < 0.05$; **$p < 0.01$; ***$p < 0.001$; ****$p < 0.0001$; Table S3.3).

3.4 Discussion

The work presented here aimed to develop an efficient system for investigating TA system function in *Mtb* and dissect potential functional redundancy or the cooperation of RelBE TA systems. We attempted to simultaneously silence three RelBE systems using CRISPRi in order to study their potential roles in carbon-mediated metabolic adaptation. The development of the knockdown mutants had variable success, with the combined *relBE* knockdown strain presenting minor silencing of all three bi-cistrons (Figure 3.2D). *PLJR-relBE1* produced the most effective

transcriptional repression following 72 hours of ATc induction, while *PLJR-relBE2* failed to exhibit any silencing of either gene in the *relBE2* operon (Figure 3.2A, B). The inconsistency of silencing efficiencies is not surprising with CRISPRi systems since transcriptional repression relies on strong binding of the dCas9 complex to its target sequence; further optimization of this system is required for more effective knockdown of multiple TA systems (132).

Improved silencing of *relBE2* along could be achieved by re-designing sgRNAs that target the bi-cistron with more effective PAM sites. With the Fortune Lab constructs, alternative sgRNAs can be designed to target the promoter region or the 5' untranslated region (UTR) of the bi-cistron. Identifying a stronger PAM site for the sgRNA could additionally improve the silencing effect of the final construct. Transcriptional repression of all three *relBE* systems could be further refined by targeting each individual gene rather than relying on the polar effect of CRISPRi. With refined genetic constructs, the improvement of transcriptional repression can be thoroughly assessed by testing a range of ATc concentrations and induction duration periods. In this study we induced the mutants with ATc for up to 72 hours, taking samples for RT-qPCR every 24 hours. *relBE2* and -*BE3* expression unexpectedly increased following 24-48 hours of ATc induction (Figure 3.2B, C). This phenomenon could be caused by improper gene targeting of the sgRNAs and subsequent increase in *relBE* gene expression simply from being exposed to ATc, which is a tetracycline derivative. The regulatory elements could naturally respond to ATc similarly to other protein synthesis-inhibiting antibiotics even though ATc lacks antibacterial activity. RelE2 and RelE3 has been previously shown to contribute to persister cell formation following gentamycin exposure, which also inhibits protein synthesis (136). Investigation of these trends are warranted if this system is used in future studies.

Testing the developed silencing system on *Mtb* metabolic activity under defined carbon sources resulted in differential responses of each knockdown mutant compared to WT *Mtb* (Figure 3.3). Each knockdown mutant resulted in significantly decreased metabolic activity under 1X TBST relative to WT, which would indicate the requirement of RelBE TA systems in *Mtb* survival under TBST. However, given that *relBE2* did not exhibit transcriptional repression, the difference in metabolic activity compared to WT cannot be directly correlated to RelBE TA systems. The reduced metabolism in TBST could be explained by general plasmid in TBST. Including an empty vector control strain in future work would help define the connection between reduced metabolic activity and *relBE* silencing under these conditions. The repression of *relBE1* expression interestingly resulted in a significant drop in resazurin reduction under cholesterol supplemented in 7H9, but the decline in metabolism is not observed with the *relBE1-3* knockdown mutant (Figure 3.3A). This finding implies a potential relationship between cholesterol metabolism and RelBE1 alone. Under single carbon sources, no differences in metabolic activity relative to WT *Mtb* were observed among the knockdown mutants (Figure 3.3B). Here we've collected evidence that does not support the hypothesis regarding RelBE TA systems contributing to *Mtb* carbon-mediated adaptation in central metabolism. Further experimentation is required to confirm TA function in relation to nutrient starvation conditions.

Overall, this study stands as a proof-of-concept for inducible gene silencing in *Mtb*. The application of this system towards dissecting the function of multiple TA systems would help the field to investigate the functional cooperativity of numerous TA loci in *Mtb* pathogenesis.

CHAPTER 4: FINAL DISCUSSION AND FUTURE DIRECTIONS

4.1 Introduction

Tuberculosis is a challenging disease to manage globally. Our efforts to discover novel therapeutics that are rapidly effective against both active and latent TB infections is restricted by our limited understanding of *Mtb* pathogenesis at various stages of the disease. The regulatory mechanisms that control *Mtb* adaptation to stresses elicited by the host immune response and work to establish persistence during latent infection have not been fully elucidated, and the complexity of such is understandably challenging to dissect. *Mtb* encodes at least 88 toxin-antitoxin systems (TA) implicated in the pathogen's ability to respond to stress conditions (69, 125). However, further investigation is needed to confidently link toxin-antitoxin system function to *Mtb* pathogenesis during infection. This thesis aimed to assess the function of the RelBE1 TA system in *in vitro* carbon-mediated metabolic adaptation. Additionally, we developed a genetic tool for studying TA system function in *Mtb* that will help to dissect the cooperative or redundnant function of multiple TA loci.

4.2 RelBE TA Systems and *Mycobacterium tuberculosis* Carbon-Mediated Metabolic Adaptation

RelBE TA systems consist of a RelE protein toxin and RelB protein antitoxin. RelE has been described to inhibit translation via ribosome-dependent RNA-cleavage when not bound to RelB (88, 89). Overexpression studies have found that RelE toxins induce growth arrest in *Mtb* following exposure to *in vitro* stresses, including carbon starvation and antibiotics (88, 110, 136). RelBE1 is genomically located next to a gene that is essential in the TCA cycle, so we investigated

the role of RelBE1 in *in vitro* carbon-mediated adaptation. We found no evidence suggesting that *relBE1* is transcriptionally coupled with the adjacent gene, *kgd*, and we did not observe transcriptional activity of *relE1* following exposure to single carbon sources. Significant variation was observed with *relBE1* expression at 1-hour timepoints and indicates transcriptional data should be measured after at least 24 hours. Increasing the number of biological replicates would also increase the statistical power of the experiment. Another limitation of this study was the reliance on transcription to detect RelBE1 activity under the *in vitro* conditions. As argued in a publication by LeRoux *et al*., transcriptional activity can be misleading when investigating the biological relevance of TA systems (80). Future work should aim to determine the physiological relevance of TA systems under defined stress conditions by prioritizing targeted proteomic analyses of RelBE TA systems and RNA sequencing to capture definitive evidence of native RelE toxin activity.

A lack of *relE1* expression under these conditions could be attributed to TA system regulatory mechanisms beyond cognate RelB1 interactions. Our lab has recently demonstrated regulation of *relBE2* via an anti-sense RNA termed *asrelE2* (137), and preliminary work revealed *trans*-regulation of *relE1* by *asrelE2* (data not shown). Work led by Dawson revealed that *relE2* was regulated by *asrelE2* unless *Mtb* was exposed to low pH conditions, where *relE2* transcription was induced (137). *relE1* expression was potentially silenced by *asrelE2* under these conditions, and other stresses like pH are required for *relE1* to be relieved from antisense regulation. Previous TA system research also revealed that antitoxins can interact with non-cognate toxins as a mechanism of regulation (138, 139). It is plausible that RelE toxins are under an intricate network of regulation to prevent unwarranted toxin activity on the bacterial cell, which explains why transcriptional activity was not observed.

RelBE1 function in *Mtb* metabolic adaptation to carbon was further characterized using growth and metabolic assays under defined carbon conditions. We compared the growth, survival, and metabolic activity between WT *Mtb and MtbΔrelE1* in carbon-supplemented 7H9 and minimal media. Differences in growth and metabolic activity between genotypes were observed following exposure to oleate and cholesterol supplement in 7H9, but no significant differences in outgrowth were found under this defined condition. These data point to RelE1 being involved in the optimal growth and metabolism of *Mtb* in the presence of lipids amongst other carbon sources. *ΔrelE1* did not influence growth, survival, or metabolism in oleate or cholesterol as single carbon sources, which could indicate that rather than RelE1 contributing to non-replicative persistence, the toxin functions to optimize *Mtb* metabolism under nutrient-rich environments. Interestingly, the *relE1* knockout presented reduced metabolic activity under nutrient starvation conditions in the form of TBST, suggestive of RelE1 being required for metabolic adaptation to carbon starvation. RelE1 did not appear to influence *Mtb* growth or viability under TBST based on OD_{600} and Log_{10} CFU/mL data. It is possible that additional RelBE systems work cooperatively with RelBE1 to contribute to overall *Mtb* survival under nutrient deprivation.

To address the potential functional redundancy or cooperativity of multiple RelBE TA systems in *Mtb*, we generated CRISPRi-mediated knockdown mutants and assessed their metabolic activity under the same defined carbon conditions. Multiple constructs were designed to target *relBE1, relBE2,* and *relBE3* individually, as well as a construct that simultaneously silences all three TA loci. The individual- and combined-knockdown mutants had variable success in silencing capabilities, with *relBE1* being the only construct with a statically significant silencing effect following induction with ATc. Though not statistically significant, the combined knockdown strain did produce some silencing activity of each gene within the three targeted loci

52

following induction. CRISPRi systems are expected to require extensive optimization since silencing efficiency depends on the sgRNA specificity to the targeted gene and an optimal PAM site for dCas9 recognition (132).

All RelE mutants were applied to resazurin reduction assays to further explore RelBE function in the *Mtb* metabolic response to carbon limitation. Interestingly, the *relBE1*-silencing mutant exhibited significantly lower metabolic activity under cholesterol-supplemented 7H9, which was not observed with *MtbΔrelE1*. Since there was slightly less resazurin reduction from *ΔrelE1*, increasing the number of biological replicates for both *ΔrelE1* and *PLJR-relBE1* resazurin assays should increase the statistical power of the comparisons and provide more apparent trends under supplement-cholesterol conditions. The resazurin reduction assays also highlighted a significant difference between WT *Mtb* and each knockdown mutant under TBST, which corresponds to our findings with *MtbΔrelE1*. However, given that one of the constructs that targets *relBE2* likely does not effectively silence the operon, the reduction in metabolic activity cannot be directly attributed to decreased *relBE* expression. Additional studies assessing *Mtb* metabolism under TBST are required to confidently correlate RelBE system function to overall metabolic adaptation and persistence.

4.3 Future Directions

This work collectively supports the hypothesis that RelBE TA systems contribute to metabolic adaptation to differential carbon sources in *Mtb*. These regulatory elements could additionally function under stress conditions that were not tested in these studies. RelBE2 has recently been shown to contribute to *Mtb* survival under low pH and nutrient starvation as well as activated macrophages, with pH-dependent negative regulation of *relE2* by *asrelE2* (137). Studies incorporating pH and nutrient starvation in combination are warranted to further investigate

RelBE1 function in *Mtb*. Future TA system research should also incorporate a combination of transcriptional, proteomic, genetic, and *in vivo* assays in order to fully dissect the physiological relevance of TA systems (Figure 4.1).
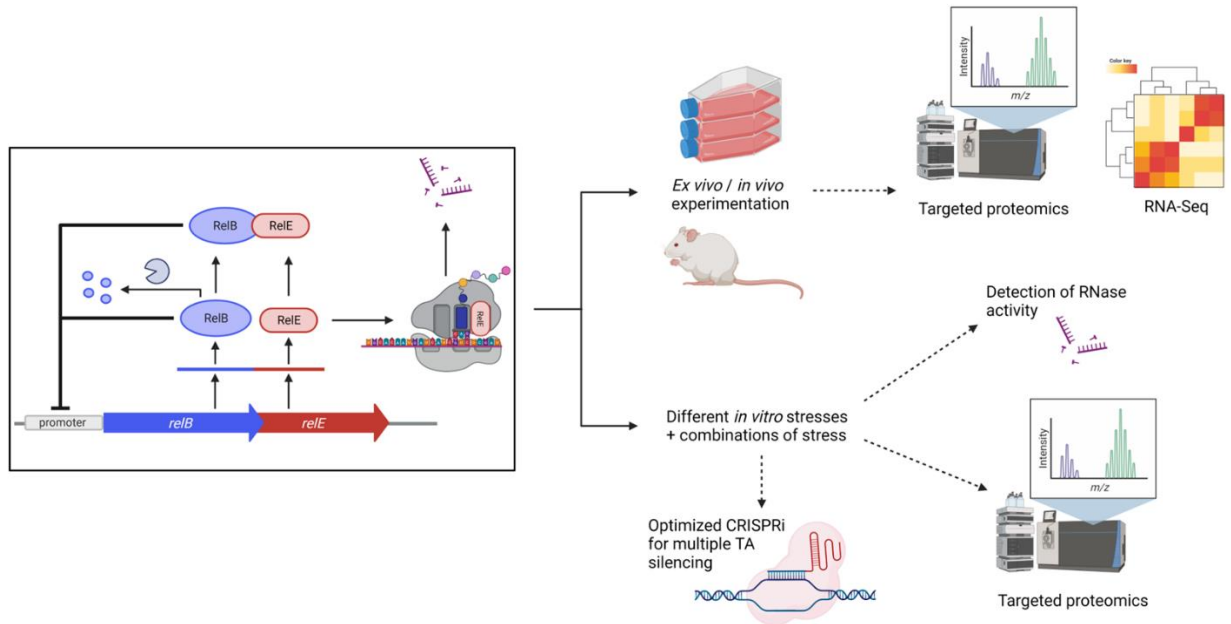
Figure 4.1 Potential routes in future *Mtb* RelBE TA system research. Further research in the function of RelBE TA systems in *Mtb* pathogenesis should include both *in vitro* and *in vivo* studies. Future studies would ideally incorporate a variety of stresses likely encountered during infection and a combination of different stresses. Nuclease activity of toxins should be detected under these conditions, and targeted proteomics should be implemented to quantify TA proteins present. CRISPRi systems targeting multiple TA loci should be included to assess the collective function of TA systems in *Mtb* stress response. *In vivo* and *ex vivo* studies are warranted to detect RelBE function during infection with the help of proteomics and RNA sequencing. Figure created with Biorender.com.

Given the current debate surrounding TA system function in persistence and stress response in prokaryotes, different hypotheses should be adequately tested. The null hypothesis for TA systems is that TA systems are nothing more than genomic "junk" that are only stable due to their addictive traits (70). In *Mtb*, the TA systems could have been acquired and maintained simply due to the lack of negative pressures. As mentioned in a study by Ramage and others, the expansion of TA systems was likely observed following the divergence of the MTBC from the last common

ancestor and thus contributes to the unique biology of species in the complex (81). Therefore, the null hypothesis seems weak when applied to *Mtb* TA systems. Another feasible hypothesis is that TA systems are largely responsible for anti-phage defense (70, 140, 141). TA system studies in *E. coli* showed phage inhibition from type I, II, III, and IV systems, and the homology of certain toxins to Cas9 proteins indicates an evolutionary link between TA systems and other anti-phage defense modules like CRISPR-Cas systems (140). Numerous mycobacteriophages have been characterized to infect mycobacteria like *Mtb*, and there is substantial evidence of co-evolution between mycobacteria and phages that resulted in CRISPR-Cas and anti-CRISPR defense systems (142). It would be interesting to explore the prevalence of phages that target *Mtb* during infection to investigate if TA systems enable the survival of *Mtb* to phages rather than host-mediated attacks.

The expansion of TA systems in *Mtb* presents a unique question that requires creative methodologies to uncover the answer. Ideally, all TA systems in *Mtb* should be knocked out to analyze potential changes in *Mtb* physiology under clinically relevant *in vitro* conditions and *in vivo*. Individual TA systems can then be introduced back into *Mtb* to effectively characterize the contribution of each TA system, each TA family, and all TA systems collectively, in *Mtb* pathogenesis. It would take a considerable amount of time to achieve, but advancements in molecular and genetic tools, including CRISPR technologies, substantially increase the feasibility of a project of that magnitude. Similar studies have been executed in other bacteria harboring multiple TA systems (80, 143). Once TA systems are confirmed to play critical roles in *Mtb* pathogenesis, clinical studies can be implemented to investigate the prevalence of these systems in drug-resistant strains. TA systems could potentially influence the susceptibility of *Mtb* to common antibiotics during infection. Work by Kazemian *et al.* performed this kind of study on 20 clinical isolates and found the expression of MazEF loci in drug-susceptible isolates (144). This

work can be expanded upon by using targeted proteomics and RNA-seq to investigate the prevalence of TA systems in a larger number of clinical isolates from regions of the world with high TB burden.

TA systems are uniquely abundant in *Mtb*, and if we can fully elucidate their individual and collective functions in *Mtb* pathogenesis, these modules would be viable targets for novel therapeutics against TB. Novel drugs can be formulated to inhibit or neutralize toxins to potentially prevent *Mtb* adaptation under stress conditions. Further research into the molecular mechanisms underlying *Mtb* adaptation and persistence is critical if we want to improve the treatment and prevention of TB disease.

LITERATURE CITED

1. World Health Organization. 2021. Global tuberculosis report 2021. World Health Organization, Geneva. https://apps.who.int/iris/handle/10665/346387. Retrieved 24 October 2021.

2. Pai M, Behr MA, Dowdy D, Dheda K, Divangahi M, Boehme CC, Ginsberg A, Swaminathan S, Spigelman M, Getahun H, Menzies D, Raviglione M. 2016. Tuberculosis. 1. Nat Rev Dis Primer 2:1–23.

3. Robertson HE. 1933. The Persistence of Tuberculous Infections. Am J Pathol 9:711-718.1.

4. McDermott W. 1959. Inapparent Infection: Relation of Latent and Dormant Infections to Microbial Persistence. The R. E. Dyer Lecture. Public Health Rep 1896-1970 74:485–499.

5. Getahun H, Matteelli A, Chaisson RE, Raviglione M. 2015. Latent Mycobacterium tuberculosis infection. N Engl J Med 372:2127–2135.

6. de Martino M, Lodi L, Galli L, Chiappini E. 2019. Immune Response to Mycobacterium tuberculosis: A Narrative Review. Front Pediatr 7:350.

7. Flynn JL, Chan J. 2001. Tuberculosis: Latency and Reactivation. Infect Immun 69:4195–4201.

8. Shea KM, Kammerer JS, Winston CA, Navin TR, Horsburgh CR. 2014. Estimated Rate of Reactivation of Latent Tuberculosis Infection in the United States, Overall and by Population Subgroup. Am J Epidemiol 179:216–225.

9. Lillebaek T, Dirksen A, Baess I, Strunge B, Thomsen VØ, Andersen ÅB. 2002. Molecular Evidence of Endogenous Reactivation of Mycobacterium tuberculosis after 33 Years of Latent Infection. J Infect Dis 185:401–404.

10. Zaman K. 2010. Tuberculosis: A Global Health Problem. J Health Popul Nutr 28:111–113.

11. Daniel TM. 2006. The history of tuberculosis. Respir Med 100:1862–1870.

12. Morse D, Brothwell DR, Ucko PJ. 1964. TUBERCULOSIS IN ANCIENT EGYPT. Am Rev Respir Dis 90:524–541.

13. Crubézy E, Ludes B, Poveda JD, Clayton J, Crouau-Roy B, Montagnon D. 1998. Identification of Mycobacterium DNA in an Egyptian Pott's disease of 5,400 years old. C R Acad Sci III 321:941–951.

14. 1946. Classic Descriptions of Disease, With Biographical Sketches of the Authors. Radiology 46:188–188.

15.   Ueber bakteriologische Forschung ; Über bakteriologische Forschung ; Vortrag in der 1. allgemeinen Sitzung des X. Internationalen Medicinischen Congresses am 4. August 1890 - Contagion - CURIOSity Digital Collections. https://curiosity.lib.harvard.edu/contagion/catalog/36-990066925910203941. Retrieved 6 June 2022.

16.   Von Pirquet C. 1909. FREQUENCY OF TUBERCULOSIS IN CHILDHOOD. J Am Med Assoc LII:675.

17.   Historical Decline of Tuberculosis in Europe and America: Its Causes and Significance | Journal of the History of Medicine and Allied Sciences | Oxford Academic. https://academic.oup.com/jhmas/article-abstract/45/3/366/709283?redirectedFrom=fulltext&login=false. Retrieved 6 June 2022.

18.   FROST WH. 1995. THE AGE SELECTION OF MORTALITY FROM TUBERCULOSIS IN SUCCESSIVE DECADES1. Am J Epidemiol 141:4–9.

19.   Calmette A. 1922. The Protection of Mankind against Tuberculosis. Edinb Med J 29:93–104.

20.   Vaccine Development Against Tuberculosis Over the Last 140 Years: Failure as Part of Success. Front Microbiol https://doi.org/10.3389/fmicb.2021.750124.

21.   Comstock GW. 1994. The International Tuberculosis Campaign: a pioneering venture in mass vaccination and research. Clin Infect Dis Off Publ Infect Dis Soc Am 19:528–540.

22.   WHO Expert Committee on Tuberculosis, Organization WH. 1974. WHO Expert Committee on Tuberculosis [meeting held in Geneva from 11 to 20 December 1973] : ninth report. World Health Organization.

23.   Zumla A, Oliver M, Sharma V, Masham S, Herbert N. 2016. World TB Day 2016—advancing global tuberculosis control efforts. Lancet Infect Dis 16:396–398.

24.   Filardo TD. 2022. Tuberculosis — United States, 2021. MMWR Morb Mortal Wkly Rep 71.

25.   Nahid P, Dorman SE, Alipanah N, Barry PM, Brozek JL, Cattamanchi A, Chaisson LH, Chaisson RE, Daley CL, Grzemska M, Higashi JM, Ho CS, Hopewell PC, Keshavjee SA, Lienhardt C, Menzies R, Merrifield C, Narita M, O'Brien R, Peloquin CA, Raftery A, Saukkonen J, Schaaf HS, Sotgiu G, Starke JR, Migliori GB, Vernon A. 2016. Executive Summary: Official American Thoracic Society/Centers for Disease Control and Prevention/Infectious Diseases Society of America Clinical Practice Guidelines: Treatment of Drug-Susceptible Tuberculosis. Clin Infect Dis 63:853–867.

26.   Carr W. 2022. Interim Guidance: 4-Month Rifapentine-Moxifloxacin Regimen for the Treatment of Drug-Susceptible Pulmonary Tuberculosis — United States, 2022. MMWR Morb Mortal Wkly Rep 71.

27.   Research C for DE and. 2019. FDA Drug Safety Communication: FDA advises restricting fluoroquinolone antibiotic use for certain uncomplicated infections; warns about disabling side effects that can occur together. FDA.

28.   Udwadia ZF. 2012. MDR, XDR, TDR tuberculosis: ominous progression. Thorax 67:286–288.

29.   Mangtani P, Abubakar I, Ariti C, Beynon R, Pimpin L, Fine PEM, Rodrigues LC, Smith PG, Lipman M, Whiting PF, Sterne JA. 2014. Protection by BCG vaccine against tuberculosis: a systematic review of randomized controlled trials. Clin Infect Dis Off Publ Infect Dis Soc Am 58:470–480.

30.   Roy A, Eisenhut M, Harris RJ, Rodrigues LC, Sridhar S, Habermann S, Snell L, Mangtani P, Adetifa I, Lalvani A, Abubakar I. 2014. Effect of BCG vaccination against Mycobacterium tuberculosis infection in children: systematic review and meta-analysis. BMJ 349:g4643.

31.   Echeverria-Valencia G, Flores-Villalva S, I.Espitia C. 2017. Virulence Factors and Pathogenicity of Mycobacterium. Mycobacterium - Res Dev https://doi.org/10.5772/intechopen.72027.

32.   Smith I. 2003. Mycobacterium tuberculosis Pathogenesis and Molecular Determinants of Virulence. Clin Microbiol Rev 16:463–496.

33.   Kirman JR, Henao-Tamayo MI, Agger EM. 2016. The Memory Immune Response to Tuberculosis. Microbiol Spectr 4.

34.   Gonzalez-Juarrero M, Kingry LC, Ordway DJ, Henao-Tamayo M, Harton M, Basaraba RJ, Hanneman WH, Orme IM, Slayden RA. 2009. Immune response to Mycobacterium tuberculosis and identification of molecular markers of disease. Am J Respir Cell Mol Biol 40:398–409.

35.   Saunders BM, Cooper AM. 2000. Restraining mycobacteria: Role of granulomas in mycobacterial infections. Immunol Cell Biol 78:334–341.

36.   Ray JCJ, Flynn JL, Kirschner DE. 2009. Synergy between Individual TNF-Dependent Functions Determines Granuloma Performance for Controlling *Mycobacterium tuberculosis* Infection. J Immunol 182:3706–3717.

37.   Fenhalls G, Stevens L, Moses L, Bezuidenhout J, Betts JC, Helden P v., Lukey PT, Duncan K. 2002. In Situ Detection of Mycobacterium tuberculosis Transcripts in Human Lung Granulomas Reveals Differential Gene Expression in Necrotic Lesions. Infect Immun 70:6330–6338.

38.   Du P, Sohaskey CD, Shi L. 2016. Transcriptional and Physiological Changes during Mycobacterium tuberculosis Reactivation from Non-replicating Persistence. Front Microbiol 7.

39.	Schnappinger D, Ehrt S, Voskuil MI, Liu Y, Mangan JA, Monahan IM, Dolganov G, Efron B, Butcher PD, Nathan C, Schoolnik GK. 2003. Transcriptional Adaptation of Mycobacterium tuberculosis within Macrophages: Insights into the Phagosomal Environment. J Exp Med 198:693–704.

40.	Ehrt S, Schnappinger D, Rhee KY. 2018. Metabolic principles of persistence and pathogenicity in Mycobacterium tuberculosis. Nat Rev Microbiol 16:496–507.

41.	Daffé M, Draper P. 1997. The Envelope Layers of Mycobacteria with Reference to their Pathogenicity, p. 131–203. *In* Poole, RK (ed.), Advances in Microbial Physiology. Academic Press.

42.	Neyrolles O, Guilhot C. 2011. Recent advances in deciphering the contribution of Mycobacterium tuberculosis lipids to pathogenesis. Tuberculosis 91:187–195.

43.	Martinot AJ, Farrow M, Bai L, Layre E, Cheng T-Y, Tsai JH, Iqbal J, Annand JW, Sullivan ZA, Hussain MM, Sacchettini J, Moody DB, Seeliger JC, Rubin EJ. 2016. Mycobacterial Metabolic Syndrome: LprG and Rv1410 Regulate Triacylglyceride Levels, Growth Rate and Virulence in Mycobacterium tuberculosis. PLoS Pathog 12:e1005351.

44.	Banerjee A, Dubnau E, Quemard A, Balasubramanian V, Um KS, Wilson T, Collins D, de Lisle G, Jacobs WR. 1994. inhA, a gene encoding a target for isoniazid and ethionamide in Mycobacterium tuberculosis. Science 263:227–230.

45.	Allué-Guardia A, García JI, Torrelles JB. 2021. Evolution of Drug-Resistant Mycobacterium tuberculosis Strains and Their Adaptation to the Human Lung Environment. Front Microbiol 12:137.

46.	Betts JC, Lukey PT, Robb LC, McAdam RA, Duncan K. 2002. Evaluation of a nutrient starvation model of Mycobacterium tuberculosis persistence by gene and protein expression profiling. Mol Microbiol 43:717–731.

47.	Griffin JE, Pandey AK, Gilmore SA, Mizrahi V, McKinney JD, Bertozzi CR, Sassetti CM. 2012. Cholesterol catabolism by Mycobacterium tuberculosis requires transcriptional and metabolic adaptations. Chem Biol 19:218–227.

48.	Deb C, Lee C-M, Dubey VS, Daniel J, Abomoelak B, Sirakova TD, Pawar S, Rogers L, Kolattukudy PE. 2009. A Novel In Vitro Multiple-Stress Dormancy Model for Mycobacterium tuberculosis Generates a Lipid-Loaded, Drug-Tolerant, Dormant Pathogen. PLOS ONE 4:e6077.

49.	Briffotaux J, Liu S, Gicquel B. 2019. Genome-Wide Transcriptional Responses of Mycobacterium to Antibiotics. Front Microbiol 10.

50.	Eoh H, Rhee K. 2014. Methylcitrate cycle defines the bactericidal essentiality of isocitrate lyase for survival of Mycobacterium tuberculosis on fatty acids. Proc Natl Acad Sci U S A 111.

51. McKinney JD, zu Bentrup KH, Muñoz-Elías EJ, Miczak A, Chen B, Chan W-T, Swenson D, Sacchettini JC, Jacobs WR, Russell DG. 2000. Persistence of Mycobacterium tuberculosis in macrophages and mice requires the glyoxylate shunt enzyme isocitrate lyase. 6797. Nature 406:735–738.

52. Tian J, Bryk R, Itoh M, Suematsu M, Nathan C. 2005. Variant tricarboxylic acid cycle in Mycobacterium tuberculosis: Identification of α-ketoglutarate decarboxylase. Proc Natl Acad Sci U S A 102:10670–10675.

53. Baker JJ, Abramovitch RB. 2018. Genetic and metabolic regulation of Mycobacterium tuberculosis acid growth arrest. 1. Sci Rep 8:4168.

54. Baker JJ, Johnson BK, Abramovitch RB. 2014. Slow growth of Mycobacterium tuberculosis at acidic pH is regulated by phoPR and host-associated carbon sources. Mol Microbiol 94:56–69.

55. Muñoz-Elías EJ, Upton AM, Cherian J, McKinney JD. 2006. Role of the methylcitrate cycle in Mycobacterium tuberculosis metabolism, intracellular growth, and virulence. Mol Microbiol 60:1109–1122.

56. Baek S-H, Li AH, Sassetti CM. 2011. Metabolic Regulation of Mycobacterial Growth and Antibiotic Sensitivity. PLOS Biol 9:e1001065.

57. Pandey AK, Sassetti CM. 2008. Mycobacterial persistence requires the utilization of host cholesterol. Proc Natl Acad Sci U S A 105:4376–4380.

58. Lee W, VanderVen BC, Fahey RJ, Russell DG. 2013. Intracellular *Mycobacterium tuberculosis* Exploits Host-derived Fatty Acids to Limit Metabolic Stress. J Biol Chem 288:6788–6800.

59. Mondino S, Cabruja M, Sala C, Cole S. FasR regulates fatty acid biosynthesis and is essential for virulence of Mycobacterium tuberculosis. BioRxiv Microbiol https://doi.org/10.1101/2020.06.08.140004.

60. de Carvalho LPS, Fischer SM, Marrero J, Nathan C, Ehrt S, Rhee KY. 2010. Metabolomics of Mycobacterium tuberculosis reveals compartmentalized co-catabolism of carbon substrates. Chem Biol 17:1122–1131.

61. Yang X, Gao J, Smith I, Dubnau E, Sampson NS. 2011. Cholesterol Is Not an Essential Source of Nutrition for Mycobacterium tuberculosis during Infection. J Bacteriol 193:1473–1476.

62. Serafini A, Tan L, Horswell S, Howell S, Greenwood DJ, Hunt DM, Phan M-D, Schembri M, Monteleone M, Montague CR, Britton W, Garza-Garcia A, Snijders AP, VanderVen B, Gutierrez MG, West NP, Carvalho LPS de. 2019. Mycobacterium tuberculosis requires glyoxylate shunt and reverse methylcitrate cycle for lactate and pyruvate metabolism. Mol Microbiol 112:1284–1307.

63. Dahl JL, Kraus CN, Boshoff HIM, Doan B, Foley K, Avarbock D, Kaplan G, Mizrahi V, Rubin H, Barry CE. 2003. The role of RelMtb-mediated adaptation to stationary phase in long-term persistence of Mycobacterium tuberculosis in mice. Proc Natl Acad Sci U S A 100:10026–10031.

64. Barker MM, Gaal T, Josaitis CA, Gourse RL. 2001. Mechanism of regulation of transcription initiation by ppGpp. I. Effects of ppGpp on transcription initiation in vivo and in vitro1 1Edited by R. Ebright. J Mol Biol 305:673–688.

65. Chang D-E, Smalley DJ, Conway T. 2002. Gene expression profiling of Escherichia coli growth transitions: an expanded stringent response model. Mol Microbiol 45:289–306.

66. Primm TP, Andersen SJ, Mizrahi V, Avarbock D, Rubin H, Barry CE. 2000. The Stringent Response of Mycobacterium tuberculosis Is Required for Long-Term Survival. J Bacteriol 182:4889–4898.

67. Sharma AK, Dhasmana N, Dubey N, Kumar N, Gangwal A, Gupta M, Singh Y. 2017. Bacterial Virulence Factors: Secreted for Survival. Indian J Microbiol 57:1–10.

68. Unterholzner SJ, Poppenberger B, Rozhon W. 2013. Toxin–antitoxin systems. Mob Genet Elem 3:e26219.

69. Page R, Peti W. 2016. Toxin-antitoxin systems in bacterial growth arrest and persistence. Nat Chem Biol 12:208–214.

70. Magnuson RD. 2007. Hypothetical Functions of Toxin-Antitoxin Systems. J Bacteriol 189:6089–6092.

71. Ogura T, Hiraga S. 1983. Mini-F plasmid genes that couple host cell division to plasmid proliferation. Proc Natl Acad Sci U S A 80:4784–4788.

72. Brzozowska I, Zielenkiewicz U. 2013. Regulation of toxin–antitoxin systems by proteolysis. Plasmid 70:33–41.

73. Jurėnas D, Fraikin N, Goormaghtigh F, Van Melderen L. 2022. Biology and evolution of bacterial toxin–antitoxin systems. 6. Nat Rev Microbiol 20:335–350.

74. Overgaard M, Borch J, Gerdes K. 2009. RelB and RelE of Escherichia coli Form a Tight Complex That Represses Transcription via the Ribbon–Helix–Helix Motif in RelB. J Mol Biol 394:183–196.

75. Cataudella I, Trusina A, Sneppen K, Gerdes K, Mitarai N. 2012. Conditional cooperativity in toxin–antitoxin regulation prevents random toxin activation and promotes fast translational recovery. Nucleic Acids Res 40:6424–6434.

76. Bøggild A, Sofos N, Andersen KR, Feddersen A, Easter AD, Passmore LA, Brodersen DE. 2012. The Crystal Structure of the Intact E. coli RelBE Toxin-Antitoxin Complex

Provides the Structural Basis for Conditional Cooperativity. Struct England1993 20:1641–1648.

77.   Wang X, Wood TK. 2011. Toxin-Antitoxin Systems Influence Biofilm and Persister Cell Formation and the General Stress Response ▽. Appl Environ Microbiol 77:5577–5583.

78.   Goormaghtigh F, Fraikin N, Putrinš M, Hallaert T, Hauryliuk V, Garcia-Pino A, Sjödin A, Kasvandik S, Udekwu K, Tenson T, Kaldalu N, Melderen LV. 2018. Reassessing the Role of Type II Toxin-Antitoxin Systems in Formation of Escherichia coli Type II Persister Cells. mBio 9.

79.   Ronneau S, Helaine S. Clarifying the Link between Toxin-Antitoxin Modules and Bacterial Persistence. J Mol Biol https://doi.org/10.1016/j.jmb.2019.03.019.

80.   LeRoux M, Culviner PH, Liu YJ, Littlehale ML, Laub MT. Stress Can Induce Transcription of Toxin-Antitoxin Systems without Activating Toxin. Mol Cell https://doi.org/10.1016/j.molcel.2020.05.028.

81.   Ramage HR, Connolly LE, Cox JS. 2009. Comprehensive Functional Analysis of Mycobacterium tuberculosis Toxin-Antitoxin Systems: Implications for Pathogenesis, Stress Responses, and Evolution. PLOS Genet 5:e1000767.

82.   Tandon H, Sharma A, Wadhwa S, Varadarajan R, Singh R, Srinivasan N, Sandhya S. 2019. Bioinformatic and mutational studies of related toxin–antitoxin pairs in *Mycobacterium tuberculosis* predict and identify key functional residues. J Biol Chem 294:9048–9063.

83.   Agarwal S, Sharma A, Bouzeyen R, Deep A, Sharma H, Mangalaparthi KK, Datta KK, Kidwai S, Gowda H, Varadarajan R, Sharma RD, Thakur KG, Singh R. VapBC22 toxin-antitoxin system from Mycobacterium tuberculosis is required for pathogenesis and modulation of host immune response. Sci Adv https://doi.org/10.1126/sciadv.aba6944.

84.   Talwar S, Pandey M, Sharma C, Kutum R, Lum J, Carbajo D, Goel R, Poidinger M, Dash D, Singhal A, Pandey AK. 2020. Role of VapBC12 Toxin-Antitoxin Locus in Cholesterol-Induced Mycobacterial Persistence. mSystems 5:e00855-20.

85.   Alexander C, Guru A, Mallick S, Mahanandia NC, Subudhi BB, Beuria TK. MazEF-rifampicin Interaction Suggests a Mechanism for Rifampicin Induced Inhibition of Persisters. Res Sq https://doi.org/10.21203/rs.3.rs-35194/v1.

86.   MazF Ribonucleases Promote Mycobacterium Tuberculosis Drug Tolerance and Virulence in Guinea Pigs - PubMed. https://pubmed.ncbi.nlm.nih.gov/25608501/. Retrieved 2 July 2020.

87.   Korch SB, Malhotra V, Contreras H, Clark-Curtiss JE. 2015. The Mycobacterium tuberculosis relBE toxin:antitoxin genes are stress-responsive modules that regulate growth through translation inhibition. J Microbiol 53:783–795.

88. Korch SB, Contreras H, Clark-Curtiss JE. 2009. Three Mycobacterium tuberculosis Rel toxin-antitoxin modules inhibit mycobacterial growth and are expressed in infected human macrophages. J Bacteriol 191:1618–1630.

89. Christensen SK, Gerdes K. 2003. RelE toxins from Bacteria and Archaea cleave mRNAs on translating ribosomes, which are rescued by tmRNA. Mol Microbiol 48:1389–1400.

90. Pedersen K, Zavialov AV, Pavlov MY, Elf J, Gerdes K, Ehrenberg M. 2003. The bacterial toxin RelE displays codon-specific cleavage of mRNAs in the ribosomal A site. Cell 112:131–140.

91. Crew R, Ramirez MV, England K, Slayden RA. 2015. MadR1, a Mycobacterium tuberculosis cell cycle stress response protein that is a member of a widely conserved protein class of prokaryotic, eukaryotic and archeal origin. Tuberc Edinb Scotl 95:251–258.

92. Adigun R, Singh R. 2020. TuberculosisStatPearls. StatPearls Publishing, Treasure Island (FL).

93. Stewart GR, Robertson BD, Young DB. 2003. Tuberculosis: a problem with persistence. Nat Rev Microbiol 1:97–105.

94. North RJ, Jung Y-J. 2004. Immunity to tuberculosis. Annu Rev Immunol 22:599–623.

95. Dutta NK, Karakousis PC. 2014. Latent Tuberculosis Infection: Myths, Models, and Molecular Mechanisms. Microbiol Mol Biol Rev MMBR 78:343–371.

96. Albors-Vaquer A, Rizvi A, Matzapetakis M, Lamosa P, Coelho AV, Patel AB, Mande SC, Gaddam S, Pineda-Lucena A, Banerjee S, Puchades-Carrasco L. 2020. Active and prospective latent tuberculosis are associated with different metabolomic profiles: clinical potential for the identification of rapid and non-invasive biomarkers. Emerg Microbes Infect 9:1131–1139.

97. Gomez JE, McKinney JD. 2004. M. tuberculosis persistence, latency, and drug tolerance. Tuberc Edinb Scotl 84:29–44.

98. Hoff DR, Ryan GJ, Driver ER, Ssemakulu CC, De Groote MA, Basaraba RJ, Lenaerts AJ. 2011. Location of Intra- and Extracellular M. tuberculosis Populations in Lungs of Mice and Guinea Pigs during Disease Progression and after Drug Treatment. PLoS ONE 6:e17550.

99. Escoll P, Buchrieser C. 2018. Metabolic reprogramming of host cells upon bacterial infection: Why shift to a Warburg-like metabolism? FEBS J 285:2146–2160.

100. Shi L, Sohaskey CD, Kana BD, Dawes S, North RJ, Mizrahi V, Gennaro ML. 2005. Changes in energy metabolism of Mycobacterium tuberculosis in mouse lung and under in vitro conditions affecting aerobic respiration. Proc Natl Acad Sci 102:15629–15634.

101. Rhee KY, Carvalho LPS de, Bryk R, Ehrt S, Marrero J, Park SW, Schnappinger D, Venugopal A, Nathan C. 2011. Central carbon metabolism in Mycobacterium tuberculosis: an unexpected frontier. Trends Microbiol 19:307–314.

102. Borah K, Mendum TA, Hawkins ND, Ward JL, Beale MH, Larrouy-Maumus G, Bhatt A, Moulin M, Haertlein M, Strohmeier G, Pichler H, Forsyth VT, Noack S, Goulding CW, McFadden J, Beste DJV. 2021. Metabolic fluxes for nutritional flexibility of Mycobacterium tuberculosis. Mol Syst Biol 17:e10280.

103. Warner DF. 2015. Mycobacterium tuberculosis Metabolism. Cold Spring Harb Perspect Med 5:a021121.

104. Maksymiuk C, Balakrishnan A, Bryk R, Rhee K, Nathan C. 2015. E1 of α-ketoglutarate dehydrogenase defends Mycobacterium tuberculosis against glutamate anaplerosis and nitroxidative stress. Proc Natl Acad Sci https://doi.org/10.1073/pnas.1510932112.

105. Wipperman MF, Sampson NS, Thomas S T. 2014. Pathogen 'Roid Rage: Cholesterol Utilization by Mycobacterium tuberculosis. Crit Rev Biochem Mol Biol 49:269–293.

106. Peyron P, Vaubourgeix J, Poquet Y, Levillain F, Botanch C, Bardou F, Daffé M, Emile J-F, Marchou B, Cardona P-J, de Chastellier C, Altare F. 2008. Foamy macrophages from tuberculous patients' granulomas constitute a nutrient-rich reservoir for M. tuberculosis persistence. PLoS Pathog 4:e1000204.

107. Russell DG, Cardona P-J, Kim M-J, Allain S, Altare F. 2009. Foamy macrophages and the progression of the human tuberculosis granuloma. Nat Immunol 10:943–948.

108. Muñoz-Elías EJ, McKinney JD. 2005. M. tuberculosis isocitrate lyases 1 and 2 are jointly required for in vivo growth and virulence. Nat Med 11:638–644.

109. Puckett S, Trujillo C, Eoh H, Marrero J, Spencer J, Jackson M, Schnappinger D, Rhee K, Ehrt S. 2014. Inactivation of Fructose-1,6-Bisphosphate Aldolase Prevents Optimal Co-catabolism of Glycolytic and Gluconeogenic Carbon Substrates in Mycobacterium tuberculosis. PLOS Pathog 10:e1004144.

110. Christensen SK, Mikkelsen M, Pedersen K, Gerdes K. 2001. RelE, a global inhibitor of translation, is activated during nutritional stress. Proc Natl Acad Sci U S A 98:14328–14333.

111. Pfaffl MW. 2001. A new mathematical model for relative quantification in real-time RT–PCR. Nucleic Acids Res 29:e45.

112. Rieu I, Powers SJ. 2009. Real-Time Quantitative RT-PCR: Design, Calculations, and Statistics. Plant Cell 21:1031–1033.

113. Bio-Rad. Measuring cytotoxicity or proliferation - alamarBlue Assay Protocol. Bio-Rad. https://www.bio-rad-antibodies.com/measuring-cytotoxicity-proliferation-spectrophotometry-fluorescence-alamarblue.html. Retrieved 18 May 2022.

114. Hershberg R, Yeger-Lotem E, Margalit H. 2005. Chromosomal organization is shaped by the transcription regulatory network. Trends Genet 21:138–142.

115. Christensen SK, Gerdes K. 2004. Delayed-relaxed response explained by hyperactivation of RelE. Mol Microbiol 53:587–597.

116. Nyka W. 1974. Studies on the Effect of Starvation on Mycobacteria. Infect Immun 9:843–850.

117. Rohde K, Yates RM, Purdy GE, Russell DG. 2007. Mycobacterium tuberculosis and the environment within the phagosome. Immunol Rev 219:37–54.

118. Muñoz-Elías EJ, Timm J, Botha T, Chan W-T, Gomez JE, McKinney JD. 2005. Replication Dynamics of Mycobacterium tuberculosis in Chronically Infected Mice. Infect Immun 73:546–551.

119. Wayne LG, Lin KY. 1982. Glyoxylate metabolism and adaptation of Mycobacterium tuberculosis to survival under anaerobic conditions. Infect Immun 37:1042–1049.

120. Zimmermann M, Kogadeeva M, Gengenbacher M, McEwen G, Mollenkopf H-J, Zamboni N, Kaufmann SHE, Sauer U. 2017. Integration of Metabolomics and Transcriptomics Reveals a Complex Diet of Mycobacterium tuberculosis during Early Macrophage Infection. mSystems 2.

121. Bellerose MM, Proulx MK, Smith CM, Baker RE, Ioerger TR, Sassetti CM. 2020. Distinct Bacterial Pathways Influence the Efficacy of Antibiotics against Mycobacterium tuberculosis. mSystems 5.

122. Bespyatykh J. 2021. Changes in the metabolism of Mycobacterium tuberculosis during the course of TB treatment. Eur Respir J 58.

123. Park H-D, Guinn KM, Harrell MI, Liao R, Voskuil MI, Tompa M, Schoolnik GK, Sherman DR. 2003. Rv3133c/dosR is a transcription factor that mediates the hypoxic response of Mycobacterium tuberculosis. Mol Microbiol 48:833–843.

124. Kang S-M, Kim D-H, Jin C, Lee B-J. 2018. A Systematic Overview of Type II and III Toxin-Antitoxin Systems with a Focus on Druggability. 12. Toxins 10:515.

125. Sala A, Bordes P, Genevaux P. 2014. Multiple Toxin-Antitoxin Systems in Mycobacterium tuberculosis. Toxins 6:1002–1020.

126. Agarwal S, Tiwari P, Deep A, Kidwai S, Gupta S, Thakur KG, Singh R. 2018. System-Wide Analysis Unravels the Differential Regulation and In Vivo Essentiality of Virulence-Associated Proteins B and C Toxin-Antitoxin Systems of Mycobacterium tuberculosis. J Infect Dis 217:1809–1820.

127. Ariyachaokun K, Grabowska AD, Gutierrez C, Neyrolles O. Multi-Stress Induction of the Mycobacterium tuberculosis MbcTA Bactericidal Toxin-Antitoxin System. Toxins https://doi.org/10.3390/toxins12050329.

128. Ramisetty BCM, Ghosh D, Roy Chowdhury M, Santhosh RS. 2016. What Is the Link between Stringent Response, Endoribonuclease Encoding Type II Toxin–Antitoxin Systems and Persistence? Front Microbiol 7.

129. Tiwari P, Arora G, Singh M, Kidwai S, Narayan OP, Singh R. 2015. MazF ribonucleases promote Mycobacterium tuberculosis drug tolerance and virulence in guinea pigs. 1. Nat Commun 6:6059.

130. Choudhary E, Thakur P, Pareek M, Agarwal N. 2015. Gene silencing by CRISPR interference in mycobacteria. 1. Nat Commun 6:6267.

131. Rock JM, Hopkins FF, Chavez A, Diallo M, Chase MR, Gerrick ER, Pritchard JR, Church GM, Rubin EJ, Sassetti CM, Schnappinger D, Fortune SM. 2017. Programmable transcriptional repression in mycobacteria using an orthogonal CRISPR interference platform. Nat Microbiol 2:16274.

132. Peters JM, Silvis MR, Zhao D, Hawkins JS, Gross CA, Qi LS. 2015. Bacterial CRISPR: Accomplishments and Prospects. Curr Opin Microbiol 27:121–126.

133. Agarwal N. Construction of a novel CRISPRi-based tool for silencing of multiple genes in Mycobacterium tuberculosis. Plasmid https://doi.org/10.1016/j.plasmid.2020.102515.

134. Wong AI, Rock JM. 2021. CRISPR Interference (CRISPRi) for Targeted Gene SilencingGene silencing in Mycobacteria, p. 343–364. *In* Parish, T, Kumar, A (eds.), Mycobacteria Protocols. Springer US, New York, NY.

135. Parish T. 2021. Electroporation of Mycobacteria, p. 273–284. *In* Parish, T, Kumar, A (eds.), Mycobacteria Protocols. Springer US, New York, NY.

136. Singh R, Barry CE, Boshoff HIM. 2010. The Three RelE Homologs of Mycobacterium tuberculosis Have Individual, Drug-Specific Effects on Bacterial Antibiotic Tolerance. J Bacteriol 192:1279–1291.

137. Dawson CC, Cummings JE, Starkey JM, Slayden RA. 2022. Discovery of a novel type IIb RelBE toxin-antitoxin system in Mycobacterium tuberculosis defined by co-regulation with an antisense RNA. Mol Microbiol https://doi.org/10.1111/mmi.14917.

138. Yang M, Gao C, Wang Y, Zhang H, He Z-G. 2010. Characterization of the Interaction and Cross-Regulation of Three Mycobacterium tuberculosis RelBE Modules. PLOS ONE 5:e10672.

139. Tu C-H, Holt M, Ruan S, Bourne C. Evaluating the Potential for Cross-Interactions of Antitoxins in Type II TA Systems. Toxins https://doi.org/10.3390/toxins12060422.

140.   Song S, Wood TK. A Primary Physiological Role of Toxin/Antitoxin Systems Is Phage Inhibition. Front Microbiol https://doi.org/10.3389/fmicb.2020.01895.

141.   Bobonis J, Mitosch K, Mateus A, Kritikos G, Elfenbein JR, Savitski MM, Andrews-Polymenis H, Typas A. Phage proteins block and trigger retron toxin/antitoxin systems. BioRxiv Microbiol https://doi.org/10.1101/2020.06.22.160242.

142.   Hatfull GF. 2018. Mycobacteriophages. Microbiol Spectr 6:10.1128/microbiolspec.GPP3-0026–2018.

143.   Tsilibaris V, Maenhaut-Michel G, Mine N, Van Melderen L. 2007. What Is the Benefit to Escherichia coli of Having Multiple Toxin-Antitoxin Systems in Its Genome? J Bacteriol 189:6101–6108.

144.   Comparison of toxin-antitoxin expression among drug-susceptible and drug-resistant clinical isolates of Mycobacterium tuberculosis. Adv Respir Med https://doi.org/475.4981.daef17fd-bdb5-487c-88d8-c7f711a87ee4.1619868415.

Chapter 2 Supplemental Tables

Supplementary Table 2.1 Primers used in experimentation.		
Gene Name	**Genome location**	**Sequence (Fwd; Rev)**
16S rRNA	MTB000019	GGTTAAGTCCCGCAACGAGC; AAGCCCTGGACATAAGGGGC
relB1	Rv1247c	AGCACCTCCAGCGTTTCCTC; AGTCCGCAATCGCCTCTCTG
relE1	Rv1246c	CTTGCCCAACCTATGCGGGT; AGCGACGACCATCCCTACCA
icl	Rv0467	ACTTCGGTGGAGAACTGGCT; GGGAACATCAGCCACATCGG
kgd	Rv1248c	GACTTCGGTGTAGTGCCGGT; GTCCCGGCCAAGCTACTGAT
glcB	Rv1837c	AGGAACTGGCGGTAGGCATC; CCAAGCTCTGTTGAACGCCC
relB2	Rv2865	CACCATCACCAAGAACGGTGC; CGTCTCCTGCAACGATTCCC
relE2	Rv2866	TCGAGACCTCCACAAGCTGC; GTGTGCTCGTCGTCAATCCG
relB3	Rv3358	AGCGCCTGTTTCCACTCATCG; CGCAGCAGATAGACCGTTTCC
relE3	Rv3357	GTTGTCGGGATACTGGTCGC; TAGTGGTATCGGGCCTTCAGC

Supplementary Table 2.2 Adjusted p-values for pairwise comparisons of *Mtb* H37Rv RT-qPCR assays. (A) p-values from Tukey's multiple comparisons following a two-way ANOVA on relative gene expression of WT *Mtb relB1* and *relE1* under single carbon source conditions. **(B)** p-values from Šidák's multiple comparisons following a two-way ANOVA on relative gene expression of *icl*, *kgd,* and *glcB* between WT and *MtbΔrelE1* under single carbon source conditions.

A. *Mtb* H37Rv *relB1* and *relE1* Expression Comparisons		
Comparison 1	**Comparison 2**	**Adjusted p-value**
relB1 Minimal Media (MM)	*relB1* MM+4mM Pyruvate	0.8632
relB1 Minimal Media (MM)	*relB1* MM+4mM Lactate	0.7888
relB1 Minimal Media (MM)	*relB1* MM+0.05mM Oleate	>0.9999
relB1 Minimal Media (MM)	*relB1* MM+0.05mM Cholesterol	0.7888
relB1 MM+4mM Pyruvate	*relB1* MM+4mM Lactate	>0.9999
relB1 MM+4mM Pyruvate	*relB1* MM+0.05mM Oleate	0.9599
relB1 MM+4mM Pyruvate	*relB1* MM+0.05mM Cholesterol	>0.9999
relB1 MM+4mM Lactate	*relB1* MM+0.05mM Oleate	0.9187
relB1 MM+4mM Lactate	*relB1* MM+0.05mM Cholesterol	>0.9999
relB1 MM+0.05mM Oleate	*relB1* MM+0.05mM Cholesterol	0.9187
relE1 Minimal Media (MM)	*relE1* MM+4mM Pyruvate	0.7436
relE1 Minimal Media (MM)	*relE1* MM+4mM Lactate	0.2870
relE1 Minimal Media (MM)	*relE1* MM+0.05mM Oleate	0.9975
relE1 Minimal Media (MM)	*relE1* MM+0.05mM Cholesterol	0.9942
relE1 MM+4mM Pyruvate	*relE1* MM+4mM Lactate	0.9887
relE1 MM+4mM Pyruvate	*relE1* MM+0.05mM Oleate	0.9863
relE1 MM+4mM Pyruvate	*relE1* MM+0.05mM Cholesterol	0.3115
relE1 MM+4mM Lactate	*relE1* MM+0.05mM Oleate	0.6444
relE1 MM+4mM Lactate	*relE1* MM+0.05mM Cholesterol	0.0846
relE1 MM+0.05mM Oleate	*relE1* MM+0.05mM Cholesterol	0.8028
B. *Mtb* H37Rv *icl*, *kgd*, and *glcB* Expression Comparisons		
Comparison 1	**Comparison 2**	**Adjusted p-value**
WT *icl* Minimal Media (MM)	*ΔrelE1 icl* Minimal Media (MM)	0.9990
WT *icl* MM+4mM Pyruvate	*ΔrelE1 icl* MM+4mM Pyruvate	0.9994
WT *icl* MM+4mM Lactate	*ΔrelE1 icl* MM+4mM Lactate	0.9999
WT *icl* MM+0.05mM Oleate	*ΔrelE1 icl* MM+0.05mM Oleate	0.9994
WT *icl* MM+0.05mM Cholesterol	*ΔrelE1 icl* MM+0.05mM Cholesterol	0.6279
WT *kgd* Minimal Media (MM)	*ΔrelE1 kgd* Minimal Media (MM)	0.9975
WT *kgd* MM+4mM Pyruvate	*ΔrelE1 kgd* MM+4mM Pyruvate	0.9891
WT *kgd* MM+4mM Lactate	*ΔrelE1 kgd* MM+4mM Lactate	0.9685
WT *kgd* MM+0.05mM Oleate	*ΔrelE1 kgd* MM+0.05mM Oleate	0.5250
WT *kgd* MM+0.05mM Cholesterol	*ΔrelE1 kgd* MM+0.05mM Cholesterol	0.9785
WT *glcB* Minimal Media (MM)	*ΔrelE1 glcB* Minimal Media (MM)	0.9764
WT *glcB* MM+4mM Pyruvate	*ΔrelE1 glcB* MM+4mM Pyruvate	0.8932
WT *glcB* MM+4mM Lactate	*ΔrelE1 glcB* MM+4mM Lactate	0.9998

WT *glcB* MM+0.05mM Oleate	*ΔrelE1 glcB* MM+0.05mM Oleate	0.9794
WT *glcB* MM+0.05mM Cholesterol	*ΔrelE1 glcB* MM+0.05mM Cholesterol	0.5554

Supplementary Table 2.3 Adjusted p-values for pairwise comparisons of *Mtb* H37Rv growth, outgrowth, and resazurin reduction assays. (A) p-values from Šídák's multiple comparisons following a two-way ANOVA on percent resazurin reduction between WT and *MtbΔrelE1*. Significant p-values are highlighted. (B) p-values from Tukey's multiple comparisons following a mixed model ANOVA on bacterial OD$_{600}$ between WT and *MtbΔrelE1* over a period of six days. (C) p-values from Tukey's multiple comparisons following a mixed model ANOVA on bacterial CFU/mL between WT and *MtbΔrelE1* over a period of six days.

A. *Mtb* H37Rv Metabolic Activity Comparisons		
Comparison 1	**Comparison 2**	**Adjusted p-value**
WT TBST	*ΔrelE1* TBST	<0.0001
WT 7H9	*ΔrelE1* 7H9	>0.9999
WT 7H9+10mM Glucose	*ΔrelE1* 7H9+10mM Glucose	>0.9999
WT 7H9+10mM Glycerol	*ΔrelE1* 7H9+10mM Glycerol	>0.9999
WT 7H9+4mM Pyruvate	*ΔrelE1* 7H9+4mM Pyruvate	>0.9999
WT 7H9+4mM Lactate	*ΔrelE1* 7H9+4mM Lactate	0.9998
WT 7H9+0.05mM Oleate	*ΔrelE1* 7H9+0.05mM Oleate	0.9108
WT 7H9+0.05mM Cholesterol	*ΔrelE1* 7H9+0.05mM Cholesterol	0.1867
WT Minimal Media (MM)	*ΔrelE1* Minimal Media (MM)	>0.9999
WT MM+10mM Glucose	*ΔrelE1* MM+10mM Glucose	>0.9999
WT MM+10mM Glycerol	*ΔrelE1* MM+10mM Glycerol	0.9997
WT MM+4mM Pyruvate	*ΔrelE1* MM+4mM Pyruvate	>0.9999
WT MM+4mM Lactate	*ΔrelE1* MM+4mM Lactate	>0.9999
WT MM+0.05mM Oleate	*ΔrelE1* MM+0.05mM Oleate	>0.9999
WT MM+0.05mM Cholesterol	*ΔrelE1* MM+0.05mM Cholesterol	0.9997

B. *Mtb* H37Rv Growth Comparisons				
Comparison 1	**Comparison 2**	**Day 2**	**Day 4**	**Day 6**
WT TBST	*ΔrelE1* TBST	0.8245	0.8971	>0.9999
WT 7H9	*ΔrelE1* 7H9	0.9992	0.9996	0.9998
WT 7H9+4mM Pyruvate	*ΔrelE1* 7H9+4mM Pyruvate	0.2575	0.2227	0.4625
WT 7H9+4mM Lactate	*ΔrelE1* 7H9+4mM Lactate	0.8973	0.6413	0.8242
WT 7H9+0.05mM Oleate	*ΔrelE1* 7H9+0.05mM Oleate	0.3342	0.4026	0.0163
WT 7H9+0.05mM Cholesterol	*ΔrelE1* 7H9+0.05mM Cholesterol	0.3268	0.2410	0.3108
WT Minimal Media (MM)	*ΔrelE1* Minimal Media (MM)	0.9884	>0.9999	0.9596
WT MM+4mM Pyruvate	*ΔrelE1* MM+4mM Pyruvate	0.8167	0.7398	0.6148
WT MM+4mM Lactate	*ΔrelE1* MM+4mM Lactate	0.7213	0.8935	0.9309
WT MM+0.05mM Oleate	*ΔrelE1* MM+0.05mM Oleate	0.9466	>0.9999	>0.9999
WT MM+0.05mM Cholesterol	*ΔrelE1* MM+0.05mM Cholesterol	0.9985	0.9997	0.9930

C. *Mtb* H37Rv Survival Comparisons				
Comparison 1	**Comparison 2**	**Day 2**	**Day 4**	**Day 6**
WT TBST	*ΔrelE1* TBST	0.9848	0.9848	0.9927
WT 7H9	*ΔrelE1* 7H9	0.9298	0.9298	0.7765
WT 7H9+4mM Pyruvate	*ΔrelE1* 7H9+4mM Pyruvate	0.6886	0.6886	>0.9999
WT 7H9+4mM Lactate	*ΔrelE1* 7H9+4mM Lactate	>0.9999	0.1878	>0.9999
WT 7H9+0.05mM Oleate	*ΔrelE1* 7H9+0.05mM Oleate	0.9851	0.9927	0.9849
WT 7H9+0.05mM Cholesterol	*ΔrelE1* 7H9+0.05mM Cholesterol	0.9914	0.9818	0.9604
WT Minimal Media (MM)	*ΔrelE1* Minimal Media (MM)	0.9912	0.4929	0.8041
WT MM+4mM Pyruvate	*ΔrelE1* MM+4mM Pyruvate	>0.9999	>0.9999	0.8644
WT MM+4mM Lactate	*ΔrelE1* MM+4mM Lactate	0.9998	0.7606	0.9164
WT MM+0.05mM Oleate	*ΔrelE1* MM+0.05mM Oleate	0.8782	0.0565	0.9411
WT MM+0.05mM Cholesterol	*ΔrelE1* MM+0.05mM Cholesterol	>0.9999	0.9574	0.9719

Chapter 3 Supplementary Tables

Supplementary Table 3.1 Primers and sgRNA oligos used in experimentation.		
Sequence Name	**Target**	**Sequence (Fwd; Rev)**
sgRNA_RelBE1	Rv1246c-47c	GGGAGCCGATGACCTGGCGTCCATC; AAACGATGGACGCCAGGTCATCGGC
sgRNA_RelBE2	Rv2865-66	GGGAACAGGACCAGATCACCATCAC; AAACGTGATGGTGATCTGGTCCTGT
sgRNA_RelBE3	Rv3357-58	GGGAACCGGAGAACGCCAGGCGGTTG; AAACCAACCGCCTGGCGTTCTCCGGT
1834_PLJR965 (131)	PLJR965	; TTCCTGTGAAGAGCCATTGATAATG
SapIGG_Primer1	*relBE2*	CTTTTTTTTTTGAATTCTCTGACCAGGGAAAATAGCC; ATTACAGCTCTTCATGCACACCCTGCCATAAAATGAC
SapIGG_Primer2	*relBE3*	ACCGACGCTCTTCAGCATCTGACCAGGGAAAATAGCC; GTGACGAGCTCTTCCCTGACACCCTGCCATAAAATGAC

Supplementary Table 3.2 Constructs used in *Mtb* experimentation.		
Plasmid	**Additional Information**	**Source and Reference**
PLJR965	Anhydrotetracycline-inducible *Mtb* silencing vector containing *Sth1* dCas9 and Kan^R	Made available by Sarah Fortune at Addgene (131)
PLJR965-relBE1	PLJR965 with *relBE1*-targeting sgRNA	This study
PLJR965-relBE2	PLJR965 with *relBE2*-targeting sgRNA	This study
PLJR965-relBE3	PLJR965 with *relBE3*-targeting sgRNA	This study
PLJR965-relBE1-3	PLJR965 with *relBE1, -2,* and *-3*-targeting sgRNAs	This study

Supplementary Table 3.3 Adjusted p-values for pairwise comparisons of *Mtb* CRISPRi mutants from RT-qPCR assays. p-values from Tukey's multiple comparisons following a two-way ANOVA on relative *relBE* expression of *PLJR* knockdown mutants before and 24-72 hours after induction.

Mutant	Comparison 1	Comparison 2	Adjusted p-value
PLJR-relBE1	-ATc	+24hr ATc	0.0528
	-ATc	+48hr ATc	0.2692
	-ATc	+72hr ATc	0.0119
PLJR-relBE2	-ATc	+24hr ATc	0.2552
	-ATc	+48hr ATc	0.0695
	-ATc	+72hr ATc	0.2858
PLJR-relBE3	-ATc	+24hr ATc	0.5614
	-ATc	+48hr ATc	0.7541
	-ATc	+72hr ATc	0.9956
PLJR-relBE1-3	-ATc	+24hr ATc	0.3890
	-ATc	+48hr ATc	0.9999
	-ATc	+72hr ATc	>0.9999

Supplementary Table 3.4 Adjusted p-values for pairwise comparisons of *Mtb* CRISPRi mutants from resazurin reduction assays. p-values from Dunnett's multiple comparisons following a two-way ANOVA on percent resazurin reduction between WT and *PLJR* knockdown mutants under **(A)** supplemented and **(B)** single carbon conditions.

A. Supplemented Carbon Conditions		
Comparison 1	**Comparison 2**	**Adjusted p-value**
WT TBST	*PLJR-relBE1* TBST	<0.0001
WT TBST	*PLJR-relBE2* TBST	<0.0001
WT TBST	*PLJR-relBE3* TBST	0.0003
WT TBST	*PLJR-relBE1-3* TBST	<0.0001
WT 7H9	*PLJR-relBE1* 7H9	>0.9999
WT 7H9	*PLJR-relBE2* 7H9	>0.9999
WT 7H9	*PLJR-relBE3* 7H9	>0.9999
WT 7H9	*PLJR-relBE1-3* 7H9	>0.9999
WT 7H9+Pyruvate	*PLJR-relBE1* 7H9+Pyruvate	0.9374
WT 7H9+Pyruvate	*PLJR-relBE2* 7H9+Pyruvate	0.8745
WT 7H9+Pyruvate	*PLJR-relBE3* 7H9+Pyruvate	0.8968
WT 7H9+Pyruvate	*PLJR-relBE1-3* 7H9+Pyruvate	0.9148
WT 7H9+Lactate	*PLJR-relBE1* 7H9+Lactate	0.9590
WT 7H9+Lactate	*PLJR-relBE2* 7H9+Lactate	0.9601
WT 7H9+Lactate	*PLJR-relBE3* 7H9+Lactate	0.9146
WT 7H9+Lactate	*PLJR-relBE1-3* 7H9+Lactate	0.8713
WT 7H9+Oleate	*PLJR-relBE1* 7H9+Oleate	0.3009
WT 7H9+Oleate	*PLJR-relBE2* 7H9+Oleate	0.7297
WT 7H9+Oleate	*PLJR-relBE3* 7H9+Oleate	>0.9999
WT 7H9+Oleate	*PLJR-relBE1-3* 7H9+Oleate	0.9955
WT 7H9+Cholesterol	*PLJR-relBE1* 7H9+Cholesterol	0.0134
WT 7H9+Cholesterol	*PLJR-relBE2* 7H9+Cholesterol	0.0666
WT 7H9+Cholesterol	*PLJR-relBE3* 7H9+Cholesterol	0.9230
WT 7H9+Cholesterol	*PLJR-relBE1-3* 7H9+Cholesterol	0.4646
WT 7H9+Glucose	*PLJR-relBE1* 7H9+Glucose	0.9935
WT 7H9+Glucose	*PLJR-relBE2* 7H9+Glucose	0.9990
WT 7H9+Glucose	*PLJR-relBE3* 7H9+Glucose	0.7802
WT 7H9+Glucose	*PLJR-relBE1-3* 7H9+Glucose	0.9958
WT 7H9+Glycerol	*PLJR-relBE1* 7H9+Glycerol	>0.9999
WT 7H9+Glycerol	*PLJR-relBE2* 7H9+Glycerol	0.9999
WT 7H9+Glycerol	*PLJR-relBE3* 7H9+Glycerol	0.9977
WT 7H9+Glycerol	*PLJR-relBE1-3* 7H9+Glycerol	0.9999
B. Single Carbon Conditions		
WT TBST	*PLJR-relBE1* TBST	0.0058
WT TBST	*PLJR-relBE2* TBST	0.0316
WT TBST	*PLJR-relBE3* TBST	0.1018
WT TBST	*PLJR-relBE1-3* TBST	0.0137
WT MM	*PLJR-relBE1* MM	>0.9999
WT MM	*PLJR-relBE2* MM	>0.9999

WT MM	*PLJR-relBE3* MM	>0.9999
WT MM	*PLJR-relBE1-3* MM	>0.9999
WT MM+Pyruvate	*PLJR-relBE1* MM+Pyruvate	0.9456
WT MM+Pyruvate	*PLJR-relBE2* MM+Pyruvate	0.9997
WT MM+Pyruvate	*PLJR-relBE3* MM+Pyruvate	0.9880
WT MM+Pyruvate	*PLJR-relBE1-3* MM+Pyruvate	0.8057
WT MM+Lactate	*PLJR-relBE1* MM+Lactate	0.1966
WT MM+Lactate	*PLJR-relBE2* MM+Lactate	0.5625
WT MM+Lactate	*PLJR-relBE3* MM+Lactate	0.2708
WT MM+Lactate	*PLJR-relBE1-3* MM+Lactate	0.0658
WT MM+Oleate	*PLJR-relBE1* MM+Oleate	0.9036
WT MM+Oleate	*PLJR-relBE2* MM+Oleate	0.6423
WT MM+Oleate	*PLJR-relBE3* MM+Oleate	0.9930
WT MM+Oleate	*PLJR-relBE1-3* MM+Oleate	0.2771
WT MM+Cholesterol	*PLJR-relBE1* MM+Cholesterol	0.5496
WT MM+Cholesterol	*PLJR-relBE2* MM+Cholesterol	0.3953
WT MM+Cholesterol	*PLJR-relBE3* MM+Cholesterol	>0.9999
WT MM+Cholesterol	*PLJR-relBE1-3* MM+Cholesterol	0.7081
WT MM+Glucose	*PLJR-relBE1* MM+Glucose	0.9869
WT MM+Glucose	*PLJR-relBE2* MM+Glucose	0.9974
WT MM+Glucose	*PLJR-relBE3* MM+Glucose	0.1486
WT MM+Glucose	*PLJR-relBE1-3* MM+Glucose	0.9998
WT MM+Glycerol	*PLJR-relBE1* MM+Glycerol	0.9988
WT MM+Glycerol	*PLJR-relBE2* MM+Glycerol	0.9556
WT MM+Glycerol	*PLJR-relBE3* MM+Glycerol	0.9965
WT MM+Glycerol	*PLJR-relBE1-3* MM+Glycerol	0.9073